A Mathematical Model of Action Potential Heterogeneity in Adult Rat Left Ventricular Myocytes

Sandeep V. Pandit,* Robert B. Clark,† Wayne R. Giles,† and Semahat S. Demir*‡

*Joint Graduate Program in Biomedical Engineering, The University of Memphis, and The University of Tennessee Health Science Center, Memphis, Tennessee, USA; †Department of Physiology and Biophysics, The University of Calgary, Calgary, Alberta, Canada; and ‡Visiting Research Faculty of Biomedical Engineering Institute, Boğaziçi University, Istanbul, Turkey

ABSTRACT Mathematical models were developed to reconstruct the action potentials (AP) recorded in epicardial and endocardial myocytes isolated from the adult rat left ventricle. The main goal was to obtain additional insight into the ionic mechanisms responsible for the transmural AP heterogeneity. The simulation results support the hypothesis that the smaller density and the slower reactivation kinetics of the Ca^{2+}-independent transient outward K^+ current (I_t) in the endocardial myocytes can account for the longer action potential duration (APD), and more prominent rate dependence in that cell type. The larger density of the Na^+ current (I_{Na}) in the endocardial myocytes results in a faster upstroke (dV/dt_{max}). This, in addition to the smaller magnitude of I_t, is responsible for the larger peak overshoot of the simulated endocardial AP. The prolonged APD in the endocardial cell also leads to an enhanced amplitude of the sustained K^+ current (I_{ss}), and a larger influx of Ca^{2+} ions via the L-type Ca^{2+} current (I_{CaL}). The latter results in an increased sarcoplasmic reticulum (SR) load, which is mainly responsible for the higher peak systolic value of the Ca^{2+} transient $[Ca^{2+}]_i$, and the resultant increase in the Na^+-Ca^{2+} exchanger (I_{NaCa}) activity, associated with the simulated endocardial AP. In combination, these calculations provide novel, quantitative insights into the repolarization process and its naturally occurring transmural variations in the rat left ventricle.

INTRODUCTION

Electrophysiological studies conducted over the past decade have revealed the so-called transmural heterogeneity, or differences in the action potential waveforms recorded in cells isolated from the epicardial and the endocardial tissues in the left ventricles of mammalian hearts (Antzelevitch et al., 1999). These include feline (Kimura et al., 1990), canine (Antzelevitch et al., 1991), rabbit (Fedida and Giles, 1991), rat (Clark et al., 1993), human (Nabauer et al., 1996), guinea pig (Bryant et al., 1997), and mouse (Guo et al., 1999; Nguyen-Tran et al., 2000). In the left ventricle, the electrophysiological properties of the epicardial and the endocardial cells differ primarily with respect to their repolarization characteristics, with the epicardial myocytes displaying shorter action potential durations (APD). The resulting transmural voltage gradient in the intact ventricular myocardium is thought to be partially responsible for the upright T-wave of the electrocardiogram (Franz et al., 1987). Epicardial and endocardial cells also respond differently to pharmacological agents and pathophysiological states. These heterogeneous responses can amplify the intrinsic electrical differences, and thereby contribute to the substrate, and/or a trigger for the development of re-entrant arrhythmias (Antzelevitch et al., 1999).

The adult rat has been widely used as an experimental model to investigate the electrical heterogeneity in the left ventricle under normal conditions (Clark et al., 1993; Shimoni et al., 1995) and pathophysiological states such as diabetes (Shimoni et al., 1995; Casis et al., 2000), thyroid dysfunction (Shimoni et al., 1995), cardiac hypertrophy (Bryant et al., 1999; Volk et al., 2001), and myocardial infarction (Qin et al., 1996; Yao et al., 1999). Endocardial myocytes isolated from healthy adult rats consistently have longer APD (Clark et al., 1993), more prominent rate-dependent effects in APD (Shimoni et al., 1995), and a larger peak overshoot (Shipsey et al., 1997; Volk et al., 2001), when compared with epicardial ones. The longer APD is important; in addition to the electrical implications it is also a significant inotropic variable in rat ventricular myocytes (Bouchard et al., 1995; Clark et al., 1996; Sah et al., 2001). It is therefore of great interest and potential significance to understand the ionic mechanisms and their interactions that underlie the intrinsic electrical heterogeneity in the healthy adult rat left ventricle.

Experimental evidence suggests that the Ca^{2+}-independent transient outward K^+ current (I_t) is an important determinant of the differences between epicardial and endocardial action potentials in most species (Campbell et al., 1995; Giles et al., 1996). The density of I_t is smaller and the recovery from inactivation kinetics slower in rat endocardial cells than epicardial ones (Clark et al., 1993; Shimoni et al., 1995). Recent experiments also suggest the existence of a transmural gradient of the Na^+ current (I_{Na}) in the rat left ventricle, with higher densities reported in the endocardium (Ashamalla et al., 2001).

One way of obtaining additional, quantitative insight into the ionic basis of the observed epicardial-endocardial differences is to develop a mathematical model of the respective membrane action potentials. The main goal of this study was to mathematically reconstruct the action potentials from adult rat left ventricular epicardial and endocardial myo-

Received for publication 6 December 2000 and in final form 14 September 2001.

Address reprint requests to Semahat S. Demir, Ph.D., Department of Biomedical Engineering, University of Memphis, 330 Engineering Technology Building, Memphis, TN 38152-3210. Tel.: 901-678-3170; Fax: 901-678-5281; E-mail: sdemir@memphis.edu.

0006-3495/01/12/3029/23 $2.00

cytes under normal conditions. Accordingly, the comprehensive, but incomplete, biophysical descriptors for the ionic currents involved in the genesis of these action potentials were utilized. The initial specific aim was to understand whether the experimentally observed differences in I_{Na} and I_t could account for the epicardial-endocardial action potential disparity. In addition, the consequences of the regional heterogeneity of the APD on ionic currents and antiporters other than I_t and I_{Na} and the effect on cardiac contractility were addressed.

MODEL DEVELOPMENT

The mathematical models for the epicardial and endocardial cells of the rat left ventricle are based on the classical formulation of Hodgkin and Huxley (1952) and are therefore somewhat similar to our previous computational work (Demir et al., 1994, 1997, 1999). The electrical equivalent circuit representing the sarcolemmal ion channels, pumps, and the Na^+-Ca^{2+} exchanger in the adult rat left ventricular cell (epicardial and endocardial) is shown in Fig. 1 *A*. This circuit is coupled with a fluid compartment (Fig. 1 *B*), which describes the changes in Na^+, K^+, and Ca^{2+} ions in the myoplasm, and the Ca^{2+} ions in the sarcoplasmic reticulum (SR). Formulations for the equations used in the model for the epicardial cell are discussed briefly in the following subsections. The endocardial cell model is based on the epicardial formulation. The main differences between these two models are clearly outlined at the end of this section, and are justified by experimental data. The complete set of equations for these two models are provided in the Appendix.

Na^+ current (I_{Na})

The inward Na^+ current (I_{Na}) is responsible for the initial upstroke of the action potential. Equations for I_{Na} are of the type first formulated by Beeler and Reuter (1977), and consist of a fast activation variable (m^3), a fast inactivation variable (h), and a slow inactivation variable (j). The steady-state activation and inactivation curves used in the model (Fig. 2 *A*) are based on recent patch clamp experiments in rat ventricular myocytes (Lee et al., 1999). The basic kinetic characteristics of I_{Na} are similar in ventricular cells across different species (Hanck, 1995). Therefore, the time constants for activation (τ_m) (Fig. 2 *B*) and inactivation (τ_h, τ_j) (Fig. 2 *C*) were adapted from the guinea pig ventricular cell model (Luo and Rudy, 1994), and were scaled for room temperature (Colatsky, 1980). The maximum Na^+ conductance (g_{Na}) was adjusted to generate an appropriate value for the action potential amplitude and the maximal upstroke velocity (dV/dt_{max}). The normalized peak current-voltage (I–V) relationship for I_{Na} is shown along with the experimental data in Fig. 2 *D* (Lee et al., 1999).

L-type Ca^{2+} current (I_{CaL})

The inward L-type Ca^{2+} current (I_{CaL}) is responsible for the plateau phase of the action potential. The Ca^{2+} ions entering the cell through these channels provide the trigger for the Ca^{2+}-induced Ca^{2+} release (CICR) from the SR (Bers and Perez-Reyes, 1999). Our formulation for I_{CaL} follows that of Nygren and co-workers (1998), and includes time- and voltage-dependent activation and inactivation, as well as Ca^{2+}-dependent inactivation. Fig. 3 *A* shows the steady-state activation and inactivation curves used in the model, which are based on data from isolated rat cells (Katsube et al., 1998). The time constants for activation (τ_d) (Fig. 3 *B*) and inactivation (τ_{f11}, τ_{f12}) are shown (Fig. 3 *C*). The formulation of τ_d is based on a recent study in rat ventricular myocytes (Sun et al., 2000). At depolarized potentials inactivation is composed of both fast (τ_{f11}) and slow (τ_{f12}) components (Katsube et al., 1998). At more hyperpolarized potentials, the fast and the slow time constants have very similar values based on monoexponential fits to recovery from inactivation data at −50 mV and −80 mV (Meszaros et al., 1997; Nawrath and Wegener, 1997). Ca^{2+}-dependent inactivation is modeled as a function of the Ca^{2+} concentration in the restricted subspace located between the junctional sarcoplasmic reticulum (JSR) and the T-tubules ($[Ca^{2+}]_{ss}$). The reversal potential for I_{CaL} (E_{CaL}) was set to a constant value of +65.0 mV, as measured experimentally (Bouchard et al., 1995), instead of the Nernst potential for the Ca^{2+} ions, as in previous models (Lindblad et al., 1996; Nygren et al., 1998). It has been shown that there is a large variation in the density of I_{CaL} in rat ventricular myocytes, even among cells from the same region (Richard et al., 1993; Gomez et al., 1997). Therefore, a normalized I–V relationship for I_{CaL} (Fig. 3 *D*) was compared to experimental data (Richard et al., 1993). I_{CaL} influences the action potential morphology (plateau) in rats. Therefore, the maximum conductance value of I_{CaL} (g_{CaL}) was adjusted so that the simulated and experimentally recorded epicardial action potential waveforms were in close agreement. The value of g_{CaL} was further constrained by making sure that the influx of Ca^{2+} ions via I_{CaL} (Q_{CaL}) during a simulated action potential was comparable to experimentally measured values (Bouchard et al., 1995).

Ca^{2+}-independent transient outward K^+ current (I_t)

In most studies of the transient outward K^+ current (I_t) in rat ventricular myocytes, Ca^{2+} channel blockers such as $CdCl_2$ or $CoCl_2$ are used to minimize the interference of I_{CaL} while recording I_t. However, divalent cations such as Co^{2+} and Cd^{2+} significantly alter the properties of I_t (Agus et al., 1991; Stengl et al., 1998a) by shifting the steady-state activation and inactivation characteristics and the voltage-dependence of the time constant for activation in the depolarized direction. Accordingly, to formulate equations for I_t under more physiological conditions, we have used experimental data for steady-state activation and inactivation (Fig. 4 *A*), which is free from this complication (Stengl et al., 1998a). Fig. 4, *B* and *C* show the time constants for activation and inactivation, respectively. The time constant for activation is based on experimental data obtained in the absence of divalent cations (Agus et al., 1991). Inactivation in I_t can be described as a sum of fast (s) and slow (s_{slow}) variables. The inactivation time constants display almost identical values at voltages positive to 0 mV (≈35 ms), and different values at voltages negative to 0 mV. This formulation is based on the fact that I_t is observed to inactivate with a monoexponential decaying time constant when elicited at depolarized potentials (Wettwer et al., 1993), whereas its recovery from inactivation kinetics is biexponential at more hyperpolarized potentials (Shimoni et al., 1995; Volk et al., 2001). Values for the fast and slow recovery time constants (at −90 mV), and their relative contributions to the total recovery of I_t were adapted from recent experiments in rat ventricular myocytes (Volk et al., 2001, Table 3). The biphasic recovery time course may suggest that I_t consists of a heterogeneous mixture of more than one type of current, as has been recently reported (Himmel et al., 1999). The differences in the properties of the components are not apparent during the onset of inactivation, but appear during reactivation, when the roles of recovery from inactivation are different. In Fig. 4 *D* the simulated I–V characteristics for I_t are shown along with experimental data (Clark et al., 1995). (Note that these characteristics were recorded in the presence of Cd^{2+}, so that appropriate shifts in the activation and inactivation characteristics are used while generating the model results for the I–V characteristics.)

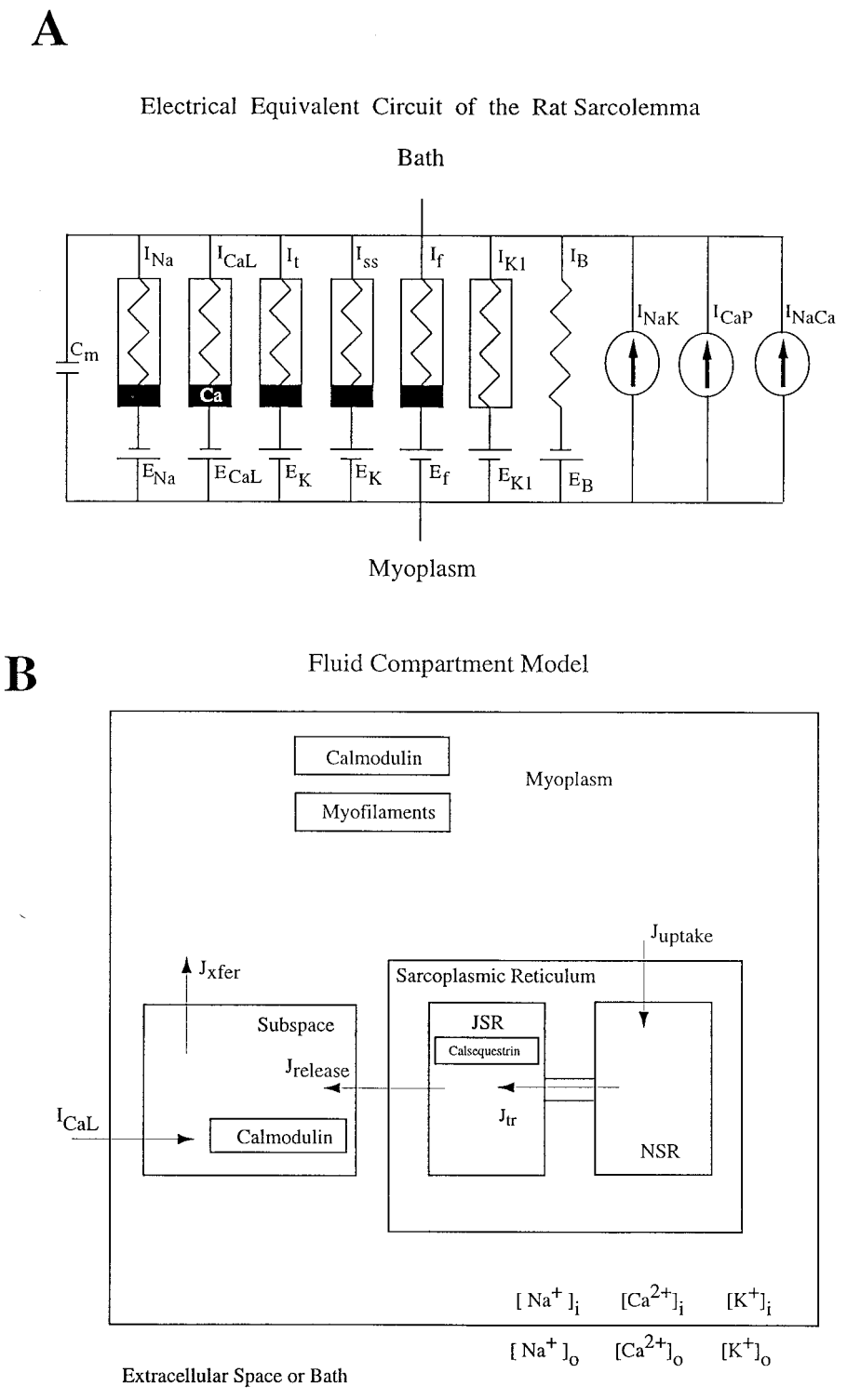

FIGURE 1 (*A*) Electrical equivalent circuit of the adult rat epicardial/endocardial ventricular cell. (*B*) Fluid compartment model of the rat cardiac cell (epi and endocardial). The expressions for the intracellular Ca^{2+} dynamics are based on the work of Winslow et al., 1999.

Steady-state outward K^+ current (I_{ss})

The steady-state outward K^+ current (I_{ss}) is characterized as a rapidly activating, very slowly inactivating current (Apkon and Nerbonne, 1991), and is also sometimes referred to as I_K in rat myocytes (Shimoni et al., 1994). Values for I_{ss} can be obtained at the end of a long (100–500 ms) depolarized voltage clamp pulse, when I_t is assumed to be completely inactivated. The steady-state activation and inactivation characteristics of I_{ss} (Fig. 5 *A*) are based on experimental data in rat ventricular myocytes (Weis et al., 1993). The time constant

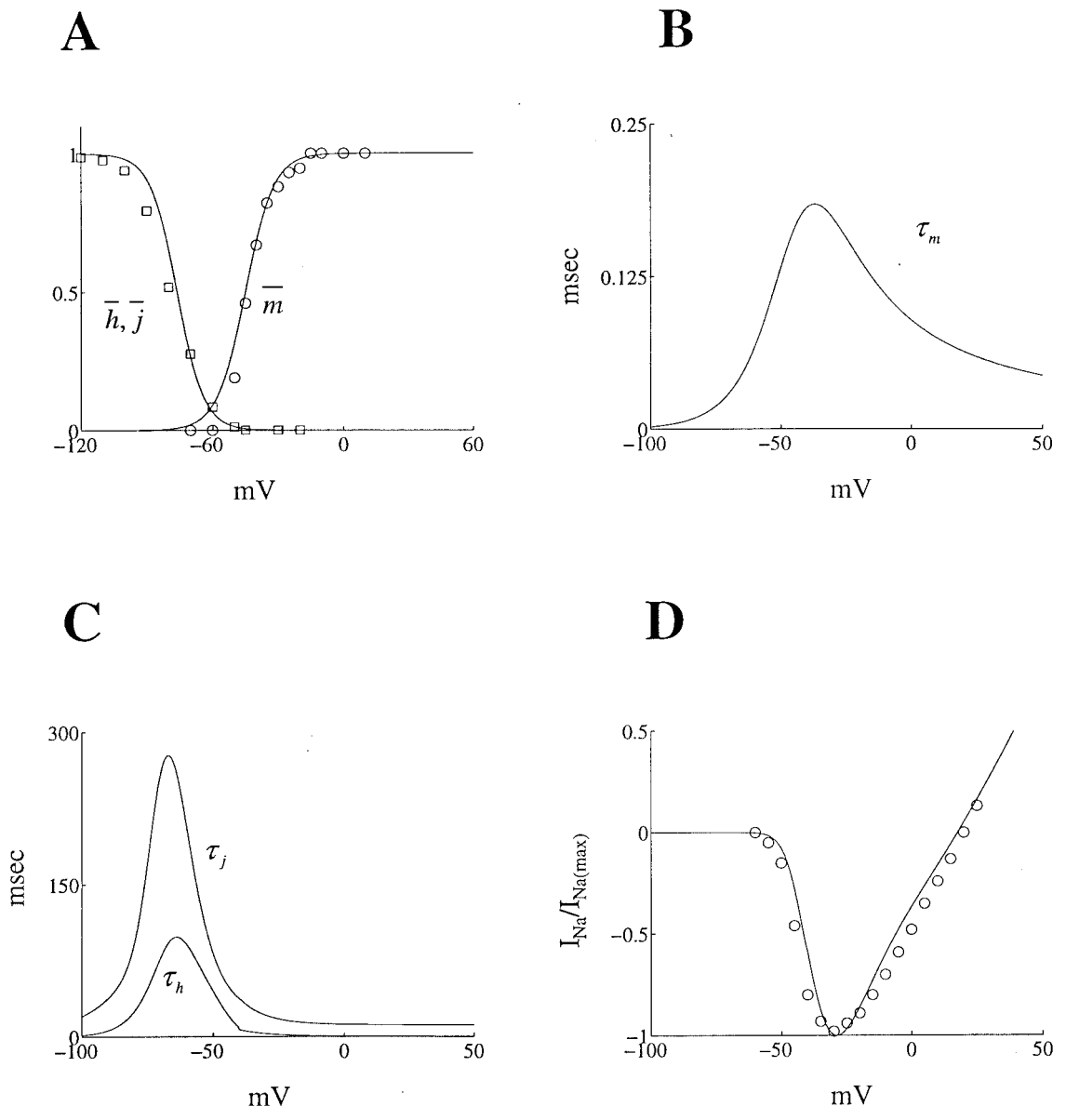

FIGURE 2 Parameters for the sodium current, I_{Na} (*A*) Steady-state activation ($\bar{m}$) and inactivation ($\bar{h}$, $\bar{j}$) (○ and □ represent data from Lee et al., 1999). (*B*) Activation time constant (τ_m) (scaled from Luo and Rudy, 1994). (*C*) Inactivation time constants (τ_h, τ_j) (scaled from Luo and Rudy, 1994). (*D*) Normalized simulated current-voltage (*I–V*) characteristics of I_{Na} (○ represents normalized data from Lee et al., 1999).

for activation (Fig. 5 *B*) is 10 times slower than the time constant for activation of I_t (Apkon and Nerbonne, 1991). The time constant for inactivation (Fig. 5 *C*) is constant (2.1 s), and is based on experimental measurements (Berger et al., 1998). In Fig. 5 *D* the model-generated *I–V* simulation of I_{ss} is compared with experimental recordings in rats (Clark et al., 1995).

Inwardly rectifying K^+ current (I_{K1})

The time-independent, inwardly rectifying K^+ current (I_{K1}) strongly modulates the resting membrane potential, and determines the input resistance of the quiescent cell. I_{K1} also contributes to the repolarization of the action potential by supplying an outward current during the late phase of repolarization. The formulation for I_{K1} was adapted from earlier work (Oehmen, 1999), and is based on data recorded from Giles' laboratory (unpublished results). The *I–V* characteristics for I_{K1} are displayed for different values of external K^+ concentrations ($[K^+]_o$) (Fig. 6 *A*).

Hyperpolarization-activated current (I_f)

A small hyperpolarization-activated inward current (I_f) was included in this model. The formulation for this current was adapted from our earlier work (Demir et al., 1994; Oehmen, 1999), and is based on data recorded in rat ventricular myocytes (Fares et al., 1998; Cerbai et al., 1996).

Background current (I_B)

The background current I_B is a sum of three linear background currents: an Na^+ current (I_{BNa}), a Ca^{2+} current (I_{BCa}), and a K^+ current (I_{BK}). These

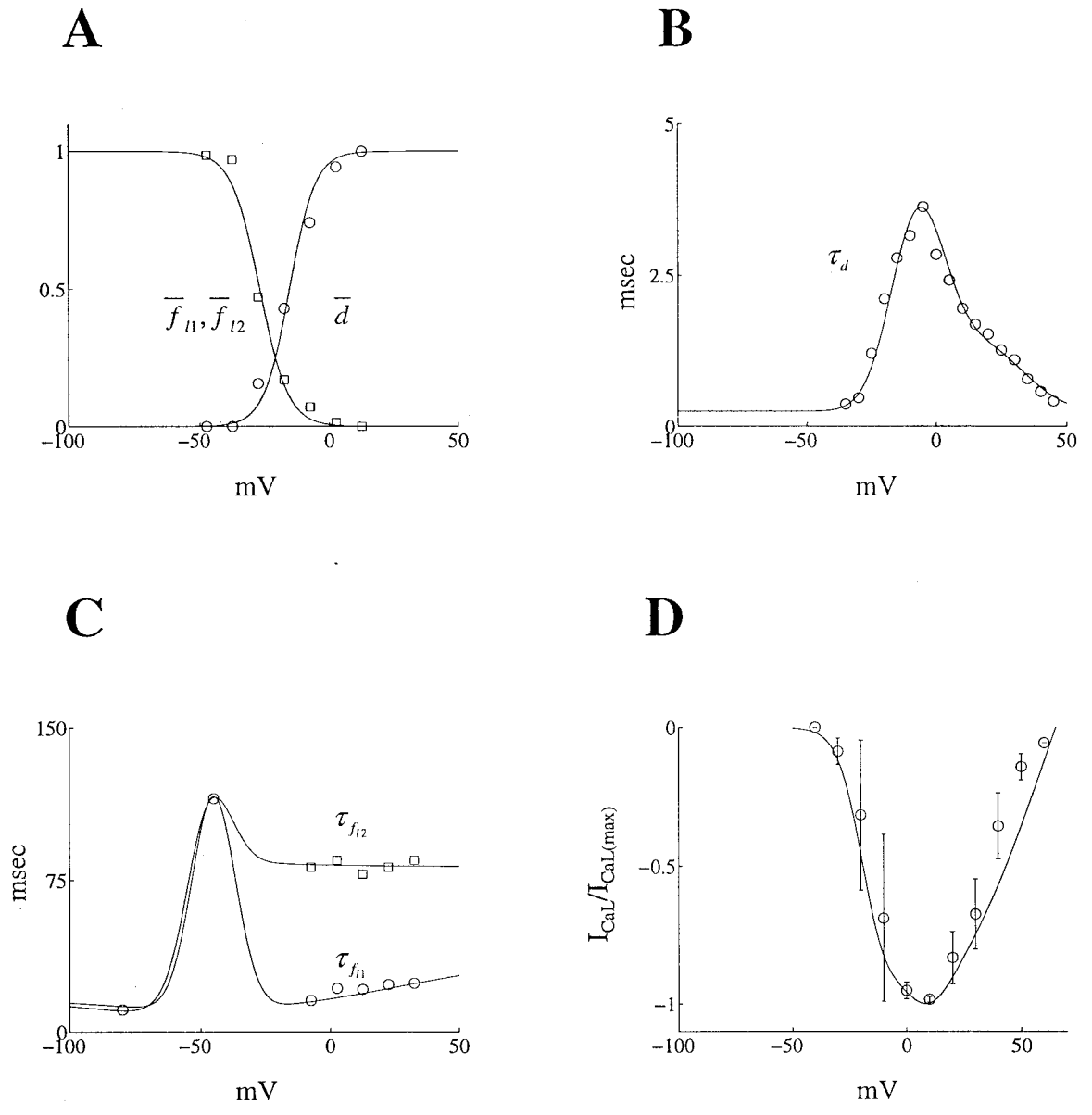

FIGURE 3 Parameters for the calcium current, I_{CaL} (*A*) Steady-state activation ($\bar{d}$) and inactivation ($\overline{f_{l1}}$, $\overline{f_{l2}}$) (○ and □ represent data from Katsube et al., 1998). (*B*) Activation time constant (τ_d) (○ represents data from Sun et al., 2000). (*C*) Inactivation time constants (τ_{f11}, τ_{f12}) (○ and □ represent data for fast and slow inactivation from Katsube et al., 1998, data at −50 mV and −80 mV being recovery from inactivation kinetics, from Meszaros et al., 1997 and Nawrath and Wegner, 1997, respectively). (*D*) Normalized simulated current-voltage (*I–V*) curve for I_{CaL} (○ represents normalized data from Richard et al., 1993).

currents represent the small leak of ions across the sarcolemma, and their magnitudes are adjusted to achieve stability of the intracellular ionic concentrations (Demir et al., 1994).

Other ionic currents

A small persistent inward Na^+ current (Saint et al., 1992), a tetrodotoxin-blockable calcium current $I_{Ca(TTX)}$, which is generated by Na^+ channels (Aggarwal et al., 1997), and a novel anionic background current (Spencer et al., 2000) have been reported in rat ventricular myocytes. We have not included these currents in this version of our model. The delayed rectifier K^+ current (I_{Kr}) has been recently reported to be present in rat ventricular myocytes, albeit at a very small density (Pond et al., 2000). Therefore it was not included in the present model.

Na^+-K^+ pump (I_{NaK}) and the Ca^{2+} pump (I_{CaP})

The Na^+-K^+ pump current (I_{NaK}) maintains the Na^+ and K^+ electrochemical gradient across the sarcolemma. The equation for I_{NaK} is based on earlier formulations (Luo and Rudy, 1994), and the maximum Na^+-K^+ pump current parameter ($\bar{I}_{NaK}$) was adjusted to achieve a stable internal Na^+ ion concentration of ≈10.74 mM. Even with this adjustment, the magnitude of the model I_{NaK} in physiological concentrations of Na^+ and K^+ ions, and a clamp potential of −40 mV, was 0.2368 pA/pF (when

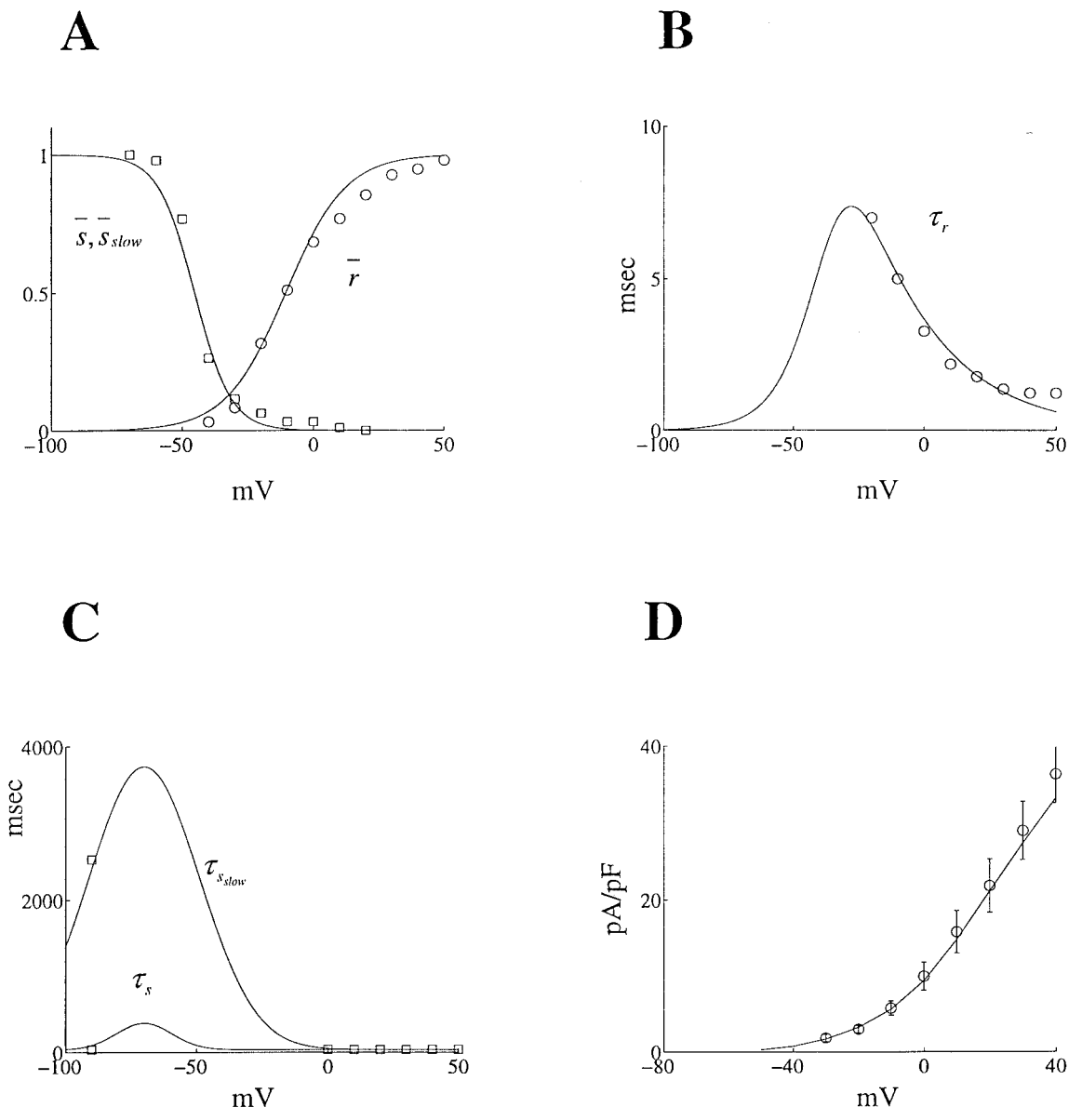

FIGURE 4 Parameters for the Ca^{2+}-independent transient outward K^+ current, I_t. (*A*) Steady-state activation ($\bar{r}$) and inactivation ($\bar{s}$, $\bar{s}_{slow}$) (○ and □ represent data recorded in the absence of divalent cations from Stengl et al., 1998a). (*B*) Activation time constant (τ_r) (○ represents data from Agus et al., 1991, recorded in the absence of divalent cations). (*C*) Inactivation time constants (τ_s, $\tau_{s_{slow}}$) (□ represents data for fast inactivation from Wettwer et al., 1993. The data for the biphasic recovery from inactivation at −90 mV is obtained from Volk et al., 2001). (*D*) Simulated current-voltage (*I–V*) curve for I_t (○ represents data from Clark et al., 1995).

normalized to 100 pF), and is within the experimentally measured range of 0.27 ± 0.05 pA/pF under identical conditions (Stimers and Dobretsov, 1998). The formulation for the Ca^{2+} pump (I_{CaP}) is based on our earlier description (Demir et al., 1994).

Na^+-Ca^{2+} exchanger (I_{NaCa})

The Na^+-Ca^{2+} exchanger current (I_{NaCa}) plays a dual role in rat ventricular myocytes. It contributes to the late repolarization phase of the action potential, and also extrudes Ca^{2+} ions from the myoplasm. The equation for I_{NaCa} was based on our earlier work (Demir et al., 1994), and the scaling factor for I_{NaCa} (k_{NaCa}) was derived from a fit to the data obtained from the *I–V* characteristics in rat ventricular myocytes (Stengl et al., 1998b) (Fig. 6 *B*); k_{NaCa} was reduced by 20% in the whole-cell model simulations to achieve intracellular Ca^{2+} homeostasis on a beat-to-beat basis.

Other pumps and exchangers

Other active ionic mechanisms in rat include the Na^+-H^+ exchanger (Wallert and Frohlich, 1989) and the Na^+-HCO_3^- cotransport mechanism (Aiello et al., 1998). We have not considered the contribution of these mechanisms to the cardiac action potential at the present time.

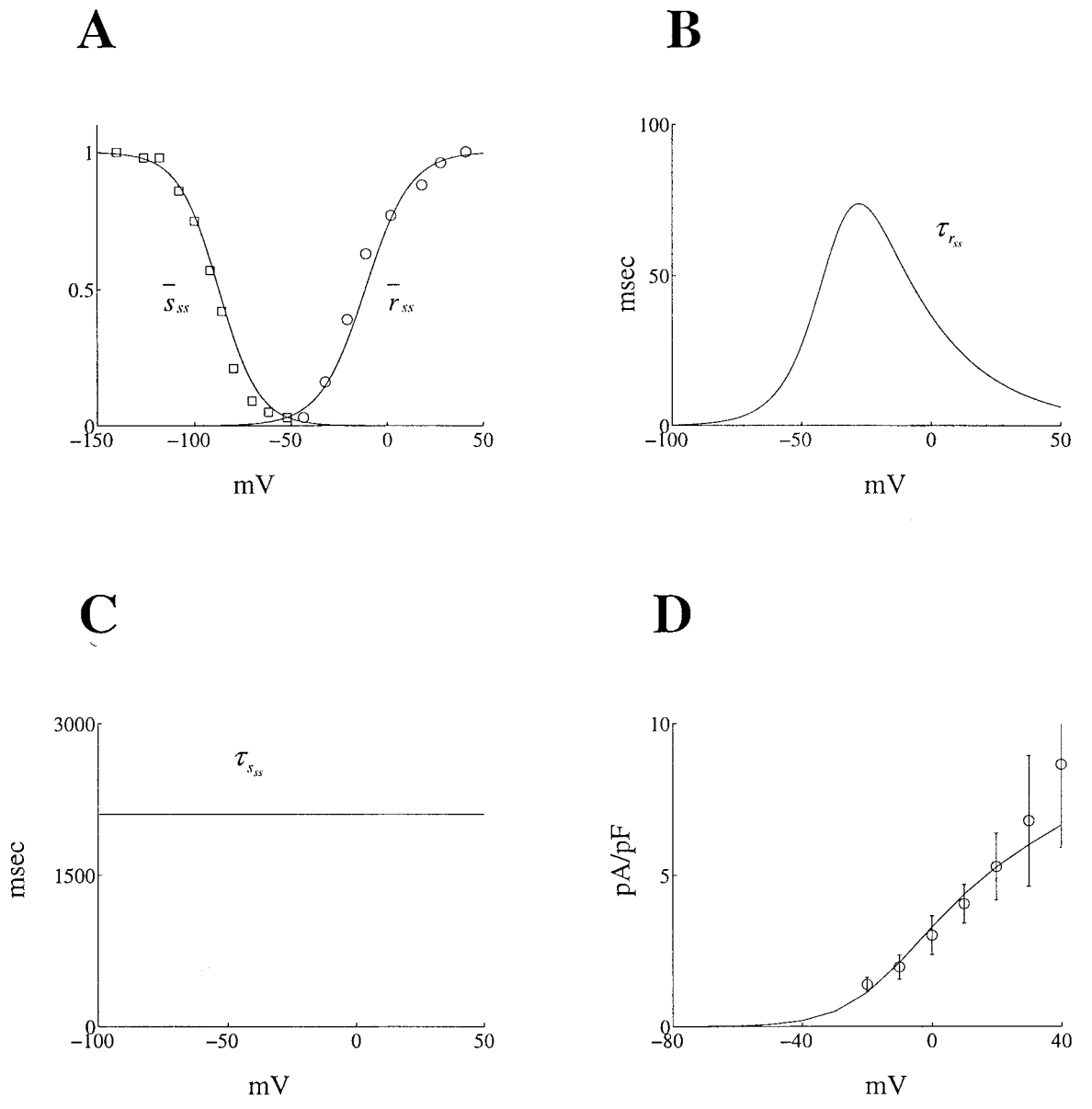

FIGURE 5 Parameters for the steady-state K^+ current, I_{ss} (*A*) Steady-state activation ($\bar{r}_{ss}$) and inactivation ($\bar{s}_{ss}$) (○ and □ represent data from Weis et al., 1993). (*B*) Activation time constant ($\tau_{r_{ss}}$), which is 10 times slower than the corresponding one for I_t (cf. Apkon and Nerbonne, 1991). (*C*) Inactivation time constant ($\tau_{s_{ss}}$) (2.1 s), not dependent membrane potential (cf. Berger et al., 1998). (*D*) Simulated current-voltage (*I–V*) curve for I_{ss}, recorded at the end of a 500-ms depolarizing voltage-clamp pulse (○ represents data recorded at the end of a 500-ms depolarizing pulse, and is obtained from Clark et al., 1995).

Intracellular and SR Ca^{2+} mechanism

The formulation for intracellular Ca^{2+} ion concentration ($[Ca^{2+}]_i$) and its various regulatory processes was adapted from a recent model of the canine midmyocardial ventricular cell (Winslow et al., 1999). The parameters for the peak forward and reverse rates of SR uptake (v_{maxf} and v_{maxr}), and the "Ca^{2+} on rate for troponin high affinity sites" (k^+_{htrpn}) were adjusted (see Appendix and Table 6 for the values in our rat ventricular cell model) to simulate a Ca^{2+} transient somewhat similar to the one observed in rats. The initial conditions for the Ca^{2+} subsystem variables in the rat model are also different from the canine ventricular cell model of Winslow et al., 1999. In particular, the values of the junctional SR and network SR are ≈0.066 mM, and comparable to the physiological values of 0.064 ± 0.006 mM, reported recently in rat ventricular myocytes (Trafford et al., 2001).

Myocyte ultrastructure

The volumes for the subcellular compartments in this model were determined from ultrastructural analysis carried out in rat ventricles (Page, 1978; Schaper et al., 1985), as described in the Appendix (Table 3). The volume and the capacitance of the cell model were assigned values of 16 pL and 100 pF, respectively, based on experimental measurements of 16 pL and 99 ± 8 pF (Bouchard et al., 1995). As a result, the model has a

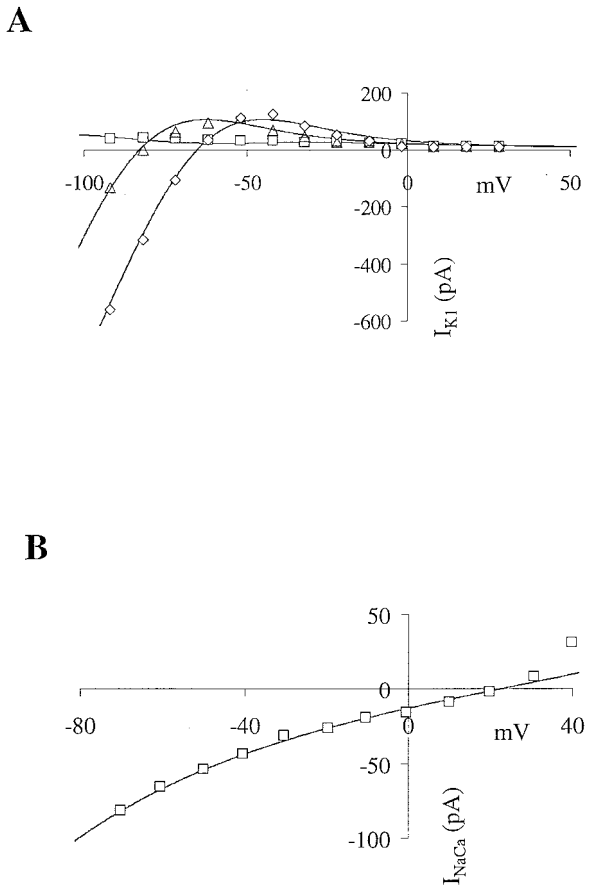

FIGURE 6 (*A*) Current-voltage (*I–V*) curve for the inwardly rectifying background K^+ current, I_{K1}, based on data from Giles' laboratory. Data for external K^+ ionic concentrations ($[K^+]_{out}$) of 10 mM (◇), 5.0 mM (△), and 1.0 mM (□) are illustrated. (*B*) Simulated *I–V* relationship for I_{NaCa}. Experimental data (○) are digitized from studies in isolated rat ventricular myocytes from Stengl et al., 1998b.

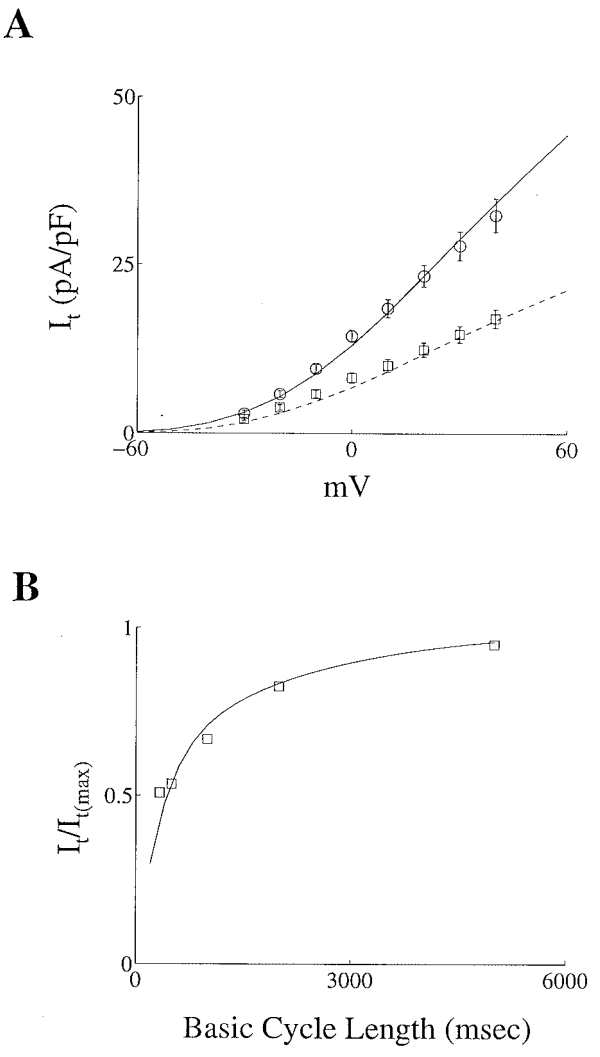

FIGURE 7 (*A*) Simulated current-voltage (*I–V*) curve for I_t in epicardial (○, *solid line*) and endocardial (□, *dashed line*) myocytes, which were isolated from the adult rat left ventricle (cf. Shimoni et al., 1995). (*B*) Simulated recovery or reactivation characteristics for I_t as a function of the basic cycle length of stimulation in the endocardial cell. □, Data obtained from the rate stimulation of I_t in rat endocardial myocytes. I_t was measured as the peak amplitude relative to zero (Shimoni et al., 1995).

capacitance-to-volume ratio of 6.25 pF/pL, similar to experimentally reported values, 6.76 ± 0.62 pF/pL (Satoh et al., 1996).

Endocardial cell model

Voltage clamp measurements in the adult rat left ventricle have shown that the density of I_t is significantly smaller, and the reactivation kinetics are much slower in the endocardial cells than the epicardial myocytes (Clark et al., 1993; Shimoni et al., 1995). However, the voltage-dependence of steady-state activation, inactivation, and the activation kinetics of I_t are similar in both epicardial and endocardial cells (Benitah et al., 1993). Thus the formulation of I_t in the endocardial model includes different equations for the fast and slow inactivation time constants, and a reduced value for the maximum conductance parameter of I_t (g_t). The reduction in g_t was estimated from experimental *I–V* data (Fig. 7 *A*) in rat epicardial and endocardial cells (Shimoni et al., 1995). Rate dependence of I_t in rat ventricular myocytes has been assessed experimentally using two different methods: 1) as the peak amplitude relative to the zero current level (I_{peak}) (Shimoni et al., 1995); and 2) as the magnitude of the transient component, i.e., the difference between the peak and the steady-state current levels ($I_{peak} - I_{ss}$) (Shimoni et al., 1995; Volk et al., 2001).

When the formulations for I_t were based on data measured using the latter approach, the model was able to reproduce the epicardial action potential rate dependence (little or no prolongation of the APD), but failed to simulate the prominent rate dependence of the endocardial action potential. Therefore, the time constants for inactivation of I_t in the endocardial cell model were based on measurements of I_t (I_{peak} only) as a function of the basic cycle length of stimulation (Fig. 7 *B*) (Shimoni et al., 1995). The densities of I_{CaL}, I_{K1}, and I_{ss} have been found to be similar in the epicardial and the endocardial regions of the rat left ventricle (Clark et al., 1993; Shimoni et al., 1995). Accordingly, the formulations for these currents are identical in the epicardial and the endocardial cell models. Recent studies have reported that the density of I_{Na} is higher by ≈33% in rat left ventricular endocardial cells than epicardial ones (Ashamalla et al., 2001). Accordingly, g_{Na} was increased in the endocardial cell model. The membrane capacitance (C_m) was assigned the same value (100 pF) in the epicardial and the endocardial cell models, based on experimental obser-

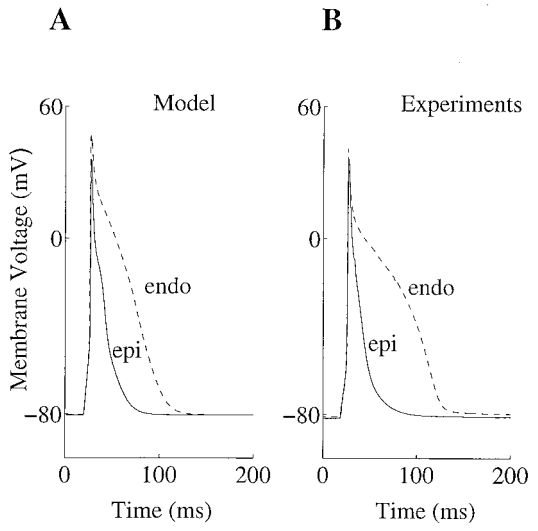

FIGURE 8 (*A*) Model generated epicardial (*solid line*) and endocardial (*dashed line*) action potentials at 1 Hz and 22°C. (*B*) Experimentally recorded epicardial (*solid line*) and endocardial (*dashed line*) action potentials (Shimoni et al., 1995).

vations (Clark et al., 1993). All other ionic mechanisms and parameters describing the SR Ca^{2+} handling were assumed to be identical in the epicardial and the endocardial models.

Basic assumptions for the models

The external ionic concentrations in both the models are assumed to be constant and all simulations were carried out at 22°C. All the results were noted in their "steady state," which was achieved by allowing the model to run for 20 s after a change in the initial conditions.

Computational aspects

The mathematical descriptors in the epicardial and/or the endocardial models consist of 28 nonlinear, first-order differential equations. A Runge-Kutta-Merson numerical integration algorithm, which includes an automatic step-size adjustment that is based on an error estimate, was used, as in our previous model simulations (Demir et al., 1994, 1997, 1999). The model equations were coded in C for the whole-cell simulations, and a SUN SPARC Ultra 60 workstation was used for all simulations. The software package Matlab was also utilized while developing equations for the individual ionic currents.

RESULTS

Simulated action potentials

A stimulus current of 0.6 nA was "applied" for 5 ms (at 1.0 Hz) to elicit the model epicardial and endocardial action potentials (Fig. 8 *A*). This is in accordance with the experimental protocol used to elicit action potentials in rat ventricular myocytes (Ward et al., 1997). The effects of the intracellular Ca^{2+} buffer EGTA have been modeled in the formulations for $[Ca^{2+}]_i$, and were adapted from a recent model (Winslow et al., 1999), and mimic the experimental

TABLE 1 Action potential characteristics in epicardial and endocardial models

	V_{rest} (mV)	R_{in} (MΩ)	dV/dt_{max} (V/s)	PO (mV)	APD_{50} (ms)	APD_{90} (ms)
Epicardial	−80.44	71.19	145.41	35.75	12.99	39.68
Endocardial	−80.37	71.32	181.41	47.08	37.83	76.43

V_{rest}, resting membrane potential; R_{in}, input resistance; dV/dt_{max}, maximum upstroke velocity; PO, peak overshoot; APD_{50}, action potential duration (50% repolarization); APD_{90}, action potential duration (90% repolarization).

recording conditions, where 10 mM EGTA was present the pipette-filling solution (Shimoni et al., 1995). Fig. 8 *B* shows representative experimental epicardial and endocardial action potential recordings (Shimoni et al., 1995). There is close agreement between the simulated and the experimentally recorded epicardial action potential waveforms. Note also that the simulated and the recorded endocardial action potentials have a prolonged APD, and a more prominent plateau phase, when compared with epicardial action potentials. The less impressive similarity of the endocardial APs is due in part to the fact that the rat endocardial action potential configuration shows a great variation in duration and shape, despite similar recording conditions (Shimoni et al., 1995; see Fig. 4, *C* and *D*). These variations might be real; i.e., due to the regional variability of the action potential waveforms within the rat endocardial wall (the base, apex, or the septum regions) (Watanabe et al., 1983). A somewhat similar and significant variability in action potential morphology has been observed in myocytes isolated from the endocardial surface of the left ventricle in ferrets (Brahmajothi et al., 1999). Accordingly, instead of attempting to closely match the simulated and experimentally recorded rat endocardial action potential morphologies by "fine tuning" the model parameters, emphasis was placed on investigating the qualitative behavior of the simulated endocardial action potential.

The characteristics of the simulated epicardial and endocardial action potentials are compared in Table 1. The resting membrane potentials (V_{rest}) for the epicardial and the endocardial cells are very similar, and in accordance with experimental recordings, which were -80.5 ± 0.5 mV and -81.3 ± 0.6 mV in the epicardial and the endocardial cells, respectively (Clark et al., 1993). The input resistances (R_{in}) of both the cells were almost identical ($\approx$71 MΩ), and are within the experimentally measured range of R_{in} values in rat ventricular cells, 62.8 ± 28.3 MΩ (Shimoni et al., 1994). R_{in} was determined by the fraction $\Delta V/\Delta I$, where ΔV was a short 5-mV hyperpolarizing pulse applied to the cell at V_{rest}, and ΔI was the resultant change in membrane current. The peak overshoot of the simulated endocardial action potential is larger than the epicardial one by 11.33 mV, and lies between the mean differences in the peak overshoot between the epicardial and the endocardial cells noted exper-

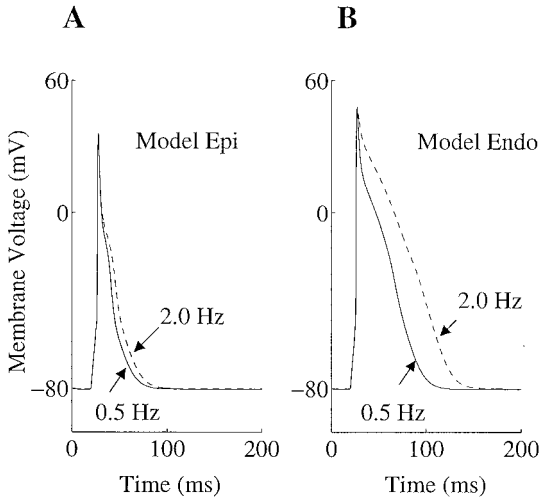

FIGURE 9 (*A*) Steady-state effects of applying stimuli on the simulated epicardial action potential at 0.5 Hz (*solid line*) and 2.0 Hz (*dashed line*). (*B*) Steady-state effects of applying stimuli on the simulated endocardial action potentials at 0.5 Hz (*solid line*) and 2.0 Hz (*dashed line*).

imentally, 10.6 mV (Volk et al., 2001), and 13.0 mV (Shipsey et al., 1997). Note from Fig. 8 *B* that the difference in the peak overshoot for the experimentally recorded epicardial and endocardial action potentials is only 3.8 mV. This is one of the reasons for the discrepancy between the simulated and this experimental endocardial action potential. The value of dV/dt_{max} is 24.76% higher in endocardial cells; this is qualitatively similar to the experimental measurements made in rat epicardial and endocardial cells (Qin et al., 1996) (The measurements in these studies were made at 37°C and under different recording conditions, and therefore cannot be compared quantitatively to model simulations.)

In Fig. 9 the frequency dependence of the simulated epicardial (panel *A*) and endocardial action potentials (panel *B*) is shown at two different frequencies, 0.5 Hz and 2.0 Hz. The model is able to reproduce 1) the more prominent rate dependence observed in the endocardial cells, and 2) exhibits little or no rate dependence in the epicardial cell simulations as observed experimentally (Shimoni et al., 1995). Note that the rate dependence of the action potentials was simulated under conditions mimicking the presence of 10 mM EGTA in the recording pipette (Shimoni et al., 1995).

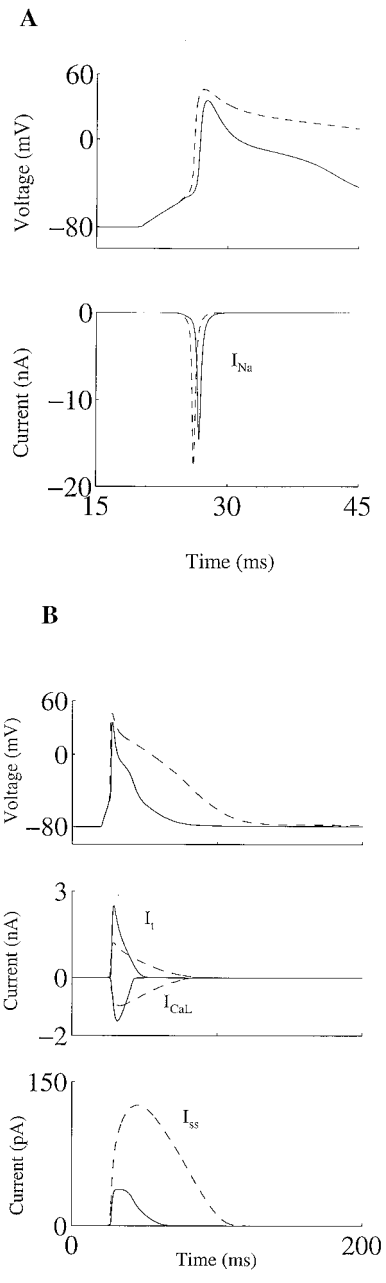

FIGURE 10 Simulated action potentials and the underlying ionic currents. (*A*) I_{Na} in the epicardial action potentials (*solid line*) and endocardial action potentials (*dashed line*). (*B*) I_{CaL}, I_t, and I_{ss} during the epicardial action potentials (*solid line*) and endocardial action potentials (*dashed line*).

Ionic mechanisms underlying the epicardial and endocardial action potentials

One approach for describing the ionic mechanisms underlying the epicardial and the endocardial action potentials is to separate the transmembrane currents that are responsible for the distinct properties of the epicardial and the endocardial action potentials (I_{Na}, I_t); and then describe the ion channels and antiporters whose behavior is significantly affected as a result of the transmural differences (I_{CaL}, I_{ss}, I_{NaCa}). Simulations for I_{Na} underlying the epicardial and the endocardial action potentials (stimulated at 1.0 Hz, in the absence of EGTA in the recording pipette, i.e., EGTA = 0 mM) are shown in Fig. 10 *A*. The larger density of I_{Na} in the endocardial cell results in a faster initial depolarization in the endocardial myocyte, and is also partially responsible for the increased peak overshoot.

TABLE 2 Calcium fluxes in epicardial and endocardial models

	Q_{CaL} (pC)	Q_{BCa} (pC)	Q_{NaCa} (pC)	$[Ca^{2+}]_{i,rest}$ (nM)	$[Ca^{2+}]_{i,peak}$ (nM)	SR_{rest} (μM)
Epicardial	14.32	4.64	18.14	78.99	357.80	66.07
Endocardial	26.38	4.51	29.55	105.32	519.09	92.34

Q_{CaL}, Calcium influx via I_{CaL} during the action potential; Q_{BCa}, Calcium influx via $I_{B,Ca}$ during the action potential; Q_{NaCa}, Calcium efflux via I_{NaCa} during the action potential; $[Ca^{2+}]_{i,rest}$, Diastolic value of $[Ca^{2+}]_i$; $[Ca^{2+}]_{i,peak}$, Peak systolic value of the Ca^{2+} transient during the action potential; SR_{rest}, JSR Ca^{2+} content during diastole.

Fig. 10 *B* shows the ionic mechanisms primarily determining the repolarization differences between the epicardial and the endocardial cells (I_t, I_{CaL}, I_{ss}). The reduction of the main repolarizing current I_t in the endocardial cell is partially responsible for the increased peak overshoot, and is also the main reason for the prolongation of the APD and the more pronounced plateau phase of the endocardial action potential. The more prominent plateau phase results in an I_{CaL} waveform, which has a smaller peak magnitude and decays more slowly. This is accompanied by an increased activation of I_{ss}, which provides additional repolarizing current during the endocardial AP.

The slowed inactivation of I_{CaL} results in an increase in the Ca^{2+} ions entering the cell via I_{CaL} (Q_{CaL}) during an endocardial action potential, as compared to the epicardial one (Table 2). Q_{CaL} for the simulated epicardial action potential (14.32 pC) is in agreement with experimentally measured values, 16.2 $\pm$ 3.0 pC (Bouchard et al., 1995). Q_{CaL} is increased by 84.22% in the endocardial cell during an identical cardiac cycle, which agrees qualitatively with recent experimental results, which showed an 110.4% increase in the mean values of Q_{CaL} for rat myocytes of endocardial origin (Volk et al., 1999). Other transmembrane currents (I_B, I_{K1}, I_{NaK}, and I_{NaCa}) underlying the epicardial and endocardial action potentials are shown in Fig. 11. The magnitude of I_f underlying the action potential is <1 pA, and hence is not shown. The small differences among I_B, I_{K1}, and I_{NaK} underlying the epicardial and endocardial action potentials are primarily due to the different time-dependent behavior of the membrane voltages between these cells. In addition to contributing to the late phase of repolarization, I_{K1} also opposes the initial depolarization of the cell membrane, and thus alters the threshold potential in both types of myocytes. I_{NaCa} underlying the epicardial and the endocardial action potentials differs in both magnitude and temporal behavior. This disparity is a result of the dependence of I_{NaCa} on membrane voltage and Ca^{2+} transient ($[Ca^{2+}]_i$). This is discussed in detail in the subsequent section. A quantitative analysis of the net Ca^{2+} fluxes across the rat sarcolemma underlying the simulated epicardial and endocardial action potentials (Table 2) reveals that the Ca^{2+} homeostasis in these cells is maintained by an almost equal amount of Ca^{2+} influx (via I_{CaL} and I_{BCa}), and efflux via I_{NaCa} during each cycle. The small discrepancy between the two can be attributed to the flux carried by I_{CaP}. The model results thus conform to the experimental observation that the exchanger (I_{NaCa}) extrudes almost the same amount of Ca^{2+} ions that enter the cardiac cell via the L-type Ca^{2+} current during each beat (Bridge et al., 1990; Bouchard et al., 1995).

TABLE 3 Cellular and subcellular volumes of rat ventricular cells

Cellular/Subcellular Organelles	Volume (pL)
Vol_{Cell}	16.00
$Vol_{nucleus}$	0.32
$Vol_{mitochondria}$	5.76
$Vol_{ss\ (subspace)}$	0.0012
Vol_{SR}	0.56
Vol_{JSR}	0.056
Vol_{NSR}	0.504
$Vol_{myo\ (myoplasm)}$ ($Vol_{myo} = Vol_{myofibrils} + Vol_{sarcoplasm}$)	9.36

TABLE 4 Standard ionic concentrations

Parameter	Definition	Value (mM)
$[K^+]_o$	Extracellular K^+ concentration	5.4
$[Na^+]_o$	Extracellular Na^+ concentration	140.0
$[Ca^{2+}]_o$	Extracellular Ca^{2+} concentration	1.2

Ca^{2+} transients in the epicardial and endocardial cell models

Simulations describing the changes in $[Ca^{2+}]_i$ underlying the epicardial and endocardial action potentials are shown in

TABLE 5 Membrane current parameters

Parameter	Definition	Value
C_m	Membrane capacitance	100e-06 μF
F	Faraday constant	96,487.0 C/mol
T	Absolute temperature	295 K
R	Ideal gas constant	8314.0 mJ/mol K
g_{Na}	Maximum conductance for I_{Na}	0.8 μS
g_{CaL}	Maximum conductance for I_{CaL}	0.031 μS
g_t	Maximum conductance for I_t	0.035 μS
g_{ss}	Maximum conductance for I_{ss}	0.007 μS
g_{K1}	Maximum conductance for I_{K1}	0.024 μS
g_{BNa}	Maximum conductance for $I_{B,Na}$	8.015e-05 μS
g_{BCa}	Maximum conductance for $I_{B,Ca}$	3.24-05 μS
g_{BK}	Maximum conductance for $I_{B,K}$	13.8e-05 μS
g_f	Maximum conductance for I_f	0.00145 μS
$\bar{I}_{NaK}$	Maximum I_{NaK} current	0.08 nA
$K_{m,Na}$	Half-maximum Na^+ binding constant for I_{NaK}	10.0 mM
$K_{m,K}$	Half-maximum K^+ binding constant for I_{NaK}	1.5 mM
$\bar{I}_{CaP}$	Maximum I_{CaP} current	0.004 nA
k_{NaCa}	Scaling factor for I_{NaCa}	0.9984e-05 $(mM)^{-4}$
d_{NaCa}	Denominator constant for I_{NaCa}	0.0001 $(mM)^{-4}$
Υ_{NaCa}	Position of energy barrier controlling voltage dependence for I_{NaCa}	0.5

TABLE 6 Parameters for describing sarcoplasmic reticulum function

Parameter	Definition	Value
v_1	Maximum RyR (ryanodine) channel Ca^{2+} flux	1.8e03 s^{-1}
K_{fb}	Forward half-saturation constant for Ca^{2+}-ATPase	0.168e-03 mM
K_{rb}	Backward half-saturation constant for Ca^{2+}-TPase	3.29 mM
K_{SR}	Scaling factor for Ca^{2+}-ATPase	1.0
N_{fb}	Forward cooperativity constant for Ca^{2+}-ATPase	1.2
N_{rb}	Reverse cooperativity constant for Ca^{2+}-ATPase	1.0
v_{maxf}	Ca^{2+}-ATPase forward rate parameter	0.4e-01 mM s^{-1}
v_{maxr}	Ca^{2+}-ATPase reverse rate parameter	0.9 mM s^{-1}
τ_{tr}	Time constant for transfer from NSR to JSR	0.5747e-03 s
τ_{xfer}	Time constant for transfer from subspace to myoplasm	26.7e-03 s
K_a^+	RyR $P_{c1} - P_{o1}$ rate constant	12.15e12 mM^{-4} s^{-1}
K_a^-	RyR $P_{o1} - P_{c1}$ rate constant	0.576e03 s^{-1}
K_b^+	RyR $P_{o1} - P_{o2}$ rate constant	4.05e09 mM^{-3} s^{-1}
K_b^-	RyR $P_{o2} - P_{o1}$ rate constant	1.930e03 s^{-1}
K_c^+	RyR $P_{o1} - P_{c2}$ rate constant	0.1e03 s^{-1}
K_c^-	RyR $P_{c2} - P_{o1}$ rate constant	0.0008e03 s^{-1}
n	RyR Ca^{2+} cooperativity parameter $P_{c1} - P_{o1}$	4
m	RyR Ca^{2+} cooperativity parameter $P_{o1} - P_{o2}$	3
$[LTRPN]_{tot}$	Total troponin low-affinity site concentration	70e-03 mM
$[HTRPN]_{tot}$	Total troponin high-affinity site concentration	140e-03 mM
K_{htrpn}^+	Ca^{2+} on rate for troponin high-affinity sites	200e03 Mm^{-1} s^{-1}
K_{htrpn}^-	Ca^{2+} off rate for troponin high-affinity sites	66.0e-03 s^{-1}
K_{1trpn}^+	Ca^{2+} on rate for troponin low-affinity sites	40e03 mM^{-1} s^{-1}
K_{1trpn}^-	Ca^{2+} on rate for troponin low-affinity sites	0.04e03 s^{-1}
$[CMDN]_{tot}$	Total myoplasm calmodulin concentration	50.0e-03 mM
$[CSQN]_{tot}$	Total myoplasm calsequestrin concentration	15.0 mM
$[EGTA]_{tot}$	Total myoplasm EGTA concentration	10.0 mM
K_m^{CMDN}	Ca^{2+} half-saturation constant for calmodulin	2.38e-03 mM
K_m^{CSQN}	Ca^{2+} half-saturation constant for calsequestrin	0.8 Mm
K_m^{EGTA}	Ca^{2+} half-saturation constant for EGTA	1.5e-04 mM

Fig. 12 *A*. The predictions of our model for the diastolic and the peak systolic values of $[Ca^{2+}]_i$ in the epicardial cell (78.99 nM and 357.80 nM, respectively) are very similar to experimental values obtained from action potential voltage clamp measurements carried out in rat ventricular myocytes, which were 79.0 ± 4.7 nM and 283 ± 44.1 nM, respectively (Kaprielian et al., 1999). The difference between the peak systolic and diastolic values of the $[Ca^{2+}]_i$ ($\Delta[Ca^{2+}]_i$), (which is sometimes considered as a more accurate estimate of the SR Ca^{2+} release, see Han et al., 1994), was 278.81 nM in the epicardial model. This is also comparable to experimental measurements obtained via field stimulation of rat cardiac myocytes, 254.0 ± 25.0 nM (McCall et al., 1998). The simulated epicardial and the endocardial Ca^{2+} transients exhibit waveforms qualitatively similar to those observed when rat myocytes were clamped by "short" and "long" action potentials, which were generated by stimulating a rat epicardial myocyte in the absence and presence of 3 mM 4-AP (a relatively selective blocker of I_t), respectively (Bouchard et al., 1995). The experimental action potentials, and the corresponding I_{CaL} and $[Ca^{2+}]_i$ waveforms, are shown in Fig. 12 *B* (Bouchard et al., 1995). The diastolic and peak systolic values of the simulated $[Ca^{2+}]_i$ for the endocardial cell are increased by 45.08% and 33.33%, respectively, compared to their epicardial counterparts (see Table 2). This is similar to experimental observations where the APD was prolonged as a result of blocking I_t (Bouchard et al., 1995), and even in rat epicardial-endocardial measurements, where an increase of 62% and 34.78% was reported for the mean diastolic and peak systolic values of $[Ca^{2+}]_i$ respectively (Figueredo et al., 1993). An increase in the amplitude of $[Ca^{2+}]_i$ also results in a corresponding increase in the magnitude of I_{NaCa} (see also Fig. 11), and is similar to the Na^+-dependent "tail current" measurements (which were representative of I_{NaCa}) in rat ventricular myocytes (Bouchard et al., 1995; Clark et al., 1996). For the $\Delta[Ca^{2+}]_i$ during a simulated epicardial action potential of 278.81 nM, the corresponding peak value of I_{NaCa} was −18.32 pA (or −0.1832 pA/pF, when normalized to model C_m of 100 pF). This agrees closely with experimental results, where peak I_{NaCa} was −0.20 ± 0.03 pA/pF for a SR Ca^{2+} release of 257 ± 42 nM (Sham et al., 1995). Thus, even though the magnitude of I_{NaCa} has been adjusted (reducing the value estimated from the *I–V* plots by 20%) to maintain Ca^{2+} balance, the peak magnitude still remains within the range of physiological measurements.

The simulated Ca^{2+} concentrations in the JSR ($[Ca^{2+}]_{JSR}$) and $[Ca^{2+}]_{ss}$ for the epicardial and endocardial cells are shown in Fig. 13. $[Ca^{2+}]_{ss}$ has peak values of 27.6 μM and 22.6 μM for epicardial and endocardial cells,

TABLE 7 Initial conditions for state variables

Variable	Definition	Initial Value
V	Membrane potential	−8.050146 + 01 mV
m	I_{Na} activation gating variable	4.164108e-03
h	I_{Na} fast inactivation gating variable	6.735613e-01
j	I_{Na} slow inactivation gating variable	6.729362e-01
d	$I_{Ca,L}$ activation gating variable	2.171081e-06
f_{11}	$I_{Ca,L}$ fast inactivation gating variable	9.999529e-01
f_{12}	$I_{Ca,L}$ slow inactivation gating variable	9.999529e-01
Ca_{inact}	Ca^{2+}-inactivation gating variable	9.913102e-01
r	I_t activation gating variable	2.191519e-03
s	I_t fast inactivation gating variable	9.842542e-01
s_{slow}	I_t slow inactivation gating variable	6.421196e-01
r_{ss}	I_{ss} activation gating variable	2.907171e-03
s_{ss}	I_{ss} inactivation gating variable	3.142767e-01
y	I_f inactivation gating variable	3.578708e-03
$[Na^+]_i$	Intracellular Na^+ concentration	1.073519e + 01 mM
$[K^+]_i$	Intracellular K^+ concentration	1.392751e + 02 mM
$[Ca^{2+}]_i$	Myoplasm Ca^{2+} concentration	7.901351e-05 mM
$[Ca^{2+}]_{NSR}$	NSR Ca^{2+} concentration	6.600742e-02 mM
$[Ca^{2+}]_{SS}$	Restricted subspace Ca^{2+} concentration	8.737212e-05 mM
$[Ca^{2+}]_{JSR}$	JSR Ca^{2+} concentration	6.607948e-02 mM
P_{C1}	Fraction of channels in state P_{C1}	6.348229e-01
P_{o1}	Fraction of channels in state P_{o1}	4.327548e-04
P_{o2}	Fraction of channels in state P_{o2}	6.062540e-10
P_{C2}	Fraction of channels in state P_{C2}	3.647471e-01
1trpn	Concentration of Ca^{2+}-bound low-affinity troponin sites	5.161900e-03 mM
htrpn	Concentration of Ca^{2+}-bound high-affinity troponin sites	1.394301e-01 mM

respectively. $[Ca^{2+}]_{ss}$ acts as the trigger for the Ca^{2+} release from the JSR. The value of $[Ca^{2+}]_{JSR}$ just before the application of the stimulus to evoke the action potentials is ≈40% higher in endocardial cells compared with epicardial cells (exact values were 66.07 μM and 92.34 μM for the epicardial and endocardial cells, respectively). The larger SR Ca^{2+} content, coupled with a larger depletion of SR during an action potential in the endocardial cell (58.5% depletion in the endocardial cell compared with 43.15% in the epicardial cell) results in a larger endocardial $[Ca^{2+}]_i$ amplitude. The increased Ca^{2+} content of SR in the presence of a longer APD in rat ventricular myocytes has been suggested earlier, based on experimental observations made via action potential voltage clamp measurements (Bouchard et al., 1995; Clark et al., 1996). Recent experiments have confirmed the occurrence of both an increased SR load and an increased fractional release of Ca^{2+} from the SR when the same rat ventricular myocyte was clamped with an action potential having a more prolonged APD (Sah et al., 2001).

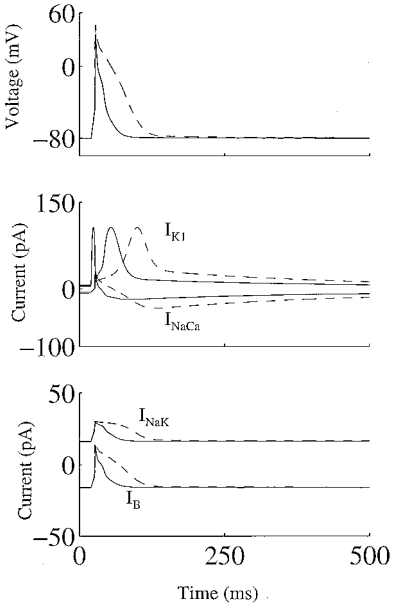

FIGURE 11 I_{K1}, I_{NaCa}, I_B, and I_{NaK} underlying epicardial action potentials (*solid line*) and endocardial action potentials (*dashed line*).

DISCUSSION

This paper describes the first successful development of a comprehensive model of the membrane action potentials in adult rat left ventricular myocytes of epi and endocardial origin. When possible, data obtained via patch clamp experiments in isolated rat cells have been utilized. A number of somewhat similar models that simulate ventricular action potentials in different species such as canine (Winslow et al., 1999), guinea pig (Nordin, 1993; Luo and Rudy, 1994; Noble et al., 1998), human (Priebe and Beuckelmann, 1998), and frog (Riemer et al., 1998) have been published

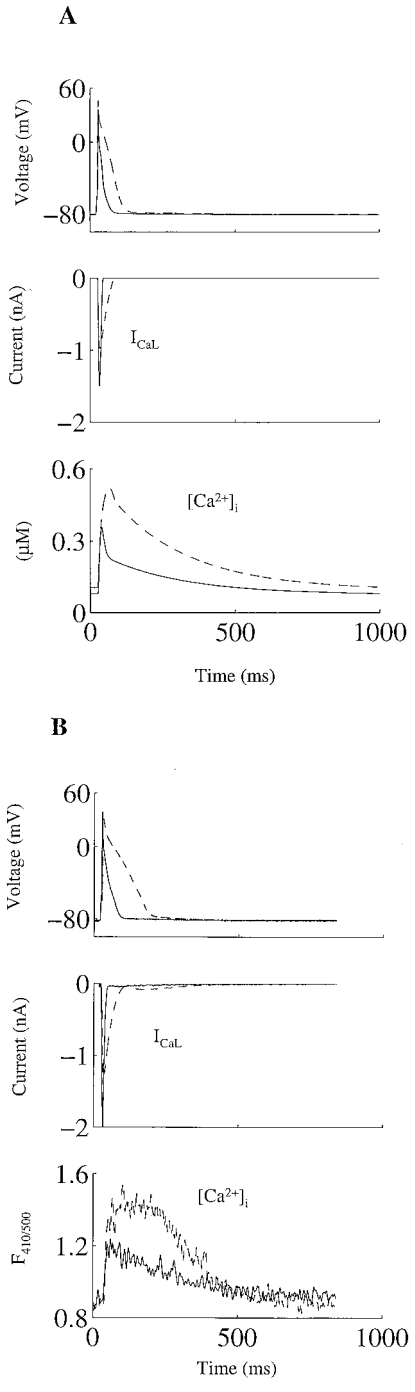

FIGURE 12 (*A*) Simulated action potentials and the underlying changes in I_{CaL} and $[Ca^{2+}]_i$ for the epicardial (*solid line*) and endocardial (*dashed line*) myocytes. (*B*) Experimentally recorded action potentials and the underlying I_{CaL} and $[Ca^{2+}]_i$ in epicardial myocytes under control conditions (*solid line*), and in the presence of 3 mM 4-AP (*dashed line*) (from Bouchard et al., 1995). Changes in the ratio of fluorescence intensity of indo 1 at 410 nm to that at 500 nm ($F_{410/500}$) were taken as a measure of changes in $[Ca^{2+}]_i$ (Bouchard et al., 1995).

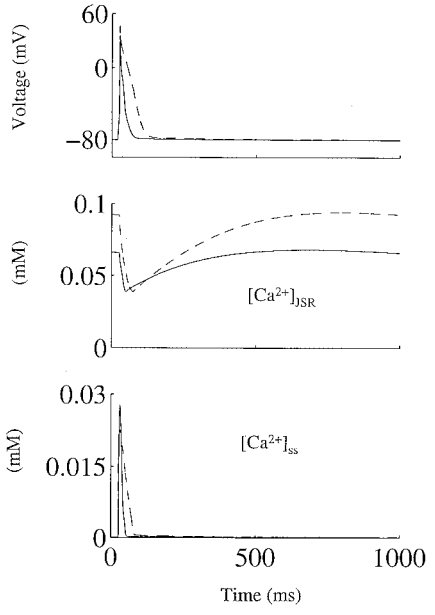

FIGURE 13 Simulated action potentials $[Ca^{2+}]_{JSR}$ and $[Ca^{2+}]_{ss}$ in epicardial (*solid line*) and endocardial (*dashed line*) cells.

during the past decade. However, there are important functional differences between the action potential waveforms in rats and other mammalian ventricular cells. Recent findings suggest that the AP in mouse may be similar to the rat AP (Gussak et al., 2000), although the detailed ionic mechanisms underlying repolarization differ quantitatively between the rat and mouse (Fiset et al., 1997b). The rat action potential has a short APD, a somewhat "triangular" shape, and shows a prolongation of the APD with an increase in the stimulus frequency (Watanabe et al., 1983; Clark et al., 1993; Shimoni et al., 1995) as opposed to a longer APD, a "spike and a dome" configuration, and a decrease in the APD in response to an increased rate of stimulus in canine and guinea pig ventricular cells (Antzelevitch et al., 1999). As expected, therefore, a comparison of the ionic currents underlying the action potentials in different species shows that they display markedly different amplitudes and time-dependent behavior as well as transmural expression pattern. I_t is absent in guinea pig ventricular cells, and the regional electrical heterogeneity in the guinea pig ventricle is mediated via the delayed rectifier (I_K) and an Na^+-dependent background current (Main et al., 1998). In addition to I_t, the transmural differences in the canine ventricle are found to be mediated via other ionic mechanisms, which include the slowly activating delayed rectifier (I_{Ks}) (Liu and Antzelevitch, 1995), a late sodium current (Eddlestone et al., 1996), and I_{NaCa} (Zygmunt et al., 2000). A new subpopulation of cells (midmyocardial "M" cells), which display a longer APD and steeper rate dependence of APD have been reported in canine (Sicouri and Antzelevitch, 1991) and guinea pig (Sicouri et al., 1996), although investigations in rat failed to provide evidence for the M cells (Shipsey et al., 1997).

The marked variation and diversity in the transmural electrophysiological characteristics across the ventricular

myocardium among mammals indicates the need for the development of rigorous species-dependent and tissue-specific (epi and endocardial) models, based on detailed experimental data and analysis. This is a requirement for a correct understanding and interpretation of the integrated behavior of the biophysical processes underlying the cardiac electrical activity of the targeted animal model in normotensive and pathophysiological conditions. The main focus of this study was the development of computational models, which could be used as a basis for investigating the ionic mechanisms of transmural heterogeneity of dispersion in repolarization, and the excitation-contraction coupling between rat myocytes of epi and endocardial origin. This was accomplished by formulating equations for the main ionic currents responsible for the genesis of the action potential, and adopting the description for the intracellular and SR Ca^{2+} dynamics from the recent work of Winslow et al., 1999. The resulting models of the epicardial and endocardial myocytes of the adult rat are able to reconstruct many of their respective action potential properties, which include the similarities (V_{rest}, R_{in}), and prominent differences (APD, peak overshoot, dV/dt_{max}, rate dependence, Q_{CaL}, Q_{NaCa}, $[Ca^{2+}]_i$, and $[Ca^{2+}]_{JSR}$). These models also offer important additional insights regarding the ionic mechanisms that underlie the epicardial and endocardial action potential heterogeneity in the adult rat left ventricle, and illustrate the interesting and highly nonlinear interactions between the major time- and voltage-dependent channel mediated currents, currents due to antiporters and/or pumps, and the small background current.

Transmural gradient of I_{Na}

The density of I_{Na} has been recently reported to be distributed nonuniformly across the rat ventricular myocardium (Ashamalla et al., 2001). Thus the density of I_{Na} is almost identical in myocytes isolated from the left ventricular endocardium and the right ventricle, but is smaller (by ≈33%) in the left ventricular epicardial myocytes. The density of I_{Na} is seen to be the sole determinant of the initial upstroke (dV/dt_{max}), whose values are similar in the simulated left ventricular endocardial and right ventricular myocyte action potentials, but faster than that in the left ventricular epicardial action potential. The present study shows that when the transmural gradients in the densities of I_{Na} and I_t (increase in I_{Na} and decrease in I_t) were incorporated in the endocardial cell model, the simulations could account for the ≈10–13 mV difference in the peak overshoot observed between the epicardial and endocardial action potentials (Shipsey et al., 1997; Volk et al., 2001). In fact, if the density of I_{Na} was not increased in the simulation of the endocardial action potential (only I_t decreased), the peak overshoot of the endocardial action potential was greater than the epicardial one by 4.92 mV only. Apparently, changes in the densities of both I_t and I_{Na} can contribute almost equally (≈5 mV each) to the larger peak overshoot in the endocardial cell. Recent experiments have reported that the density of I_t in the isolated rat right ventricular myocytes is ≈25% greater than that in isolated rat left ventricular epicardial myocytes (Casis et al., 1998). When the left ventricular epicardial cell model was modified to simulate the action potential (not shown) in right ventricular myocytes (increased I_{Na} and increased I_t), the model's predicted values for V_{rest}, dV/dt_{max}, and peak overshoot were −80.42 mV, 181.91 V/s, and 41.44 mV, respectively. These values are in close agreement with experimental measurements carried out in rat myocytes isolated from the right ventricle, which were −80.74 ± 0.57 mV, 193.25 ± 13.94 V/s, and 37.47 ± 3.21 mV, respectively (MacDonnell et al., 1998).

The simulation results thus provide a mechanistic linkage between the transmural gradient of I_{Na} and the corresponding changes in the peak overshoot and dV/dt_{max}, and underline the integrative utility of our model when one considers the fact that all three characteristics (transmural gradient of I_{Na}, differences in peak overshoot, and dV/dt_{max}) were reported in a separate set of experiments, and from different laboratories.

Formulation and function of I_t

The available experimental data and our model simulations show that I_t is almost an order of magnitude larger than the other K^+ currents (I_{ss}, I_{K1}) in both epi and endocardial myocytes; thus it is the dominant repolarizing current in both cell types. Our model simulations demonstrate that the differential density of expression and the differences in the reactivation kinetics of I_t clearly underlie the regional variations in APD and rate dependence, thus corroborating important experimental observations (Shimoni et al., 1995) with an in silico approach. This insight is important because during patch clamp experiments the properties of I_t are often studied in the presence of divalent cations, which alter the characteristics of I_t by shifting the steady-state activation and inactivation, and the voltage-dependence of the time constant for activation in the depolarized direction (Agus et al., 1991). The computational model allows one to investigate the role of I_t in a virtual cellular environment, and in interaction with other ionic currents, without altering the intrinsic properties of I_t. The half-maximal voltages of the steady-state activation ($V_{1/2,act}$) and inactivation ($V_{1/2,inact}$) for I_t in the rat models were −10.6 mV and −45.3 mV, respectively. Interestingly, these values are comparable to the corresponding values for the heterologously expressed voltage-gated K^+ channel α-subunits Kv4.2 and Kv1.4 which, along with some other α- and β-subunits, are deemed to constitute the putative molecular correlates of I_t (Oudit et al., 2001). $V_{1/2,act}$ was −13.0 ± 2.0 mV (Diochot et al., 1999), and −7.7 ± 5.4 mV (Wickenden et al., 1999a) for Kv4.2 and Kv1.4, respectively; $V_{1/2,inact}$ was −45.0 ±

3.0 mV (Fiset et al., 1997a) and −49.3 ± 1.4 mV (Wickenden et al., 1999a) for Kv4.2 and Kv1.4, respectively. Furthermore, the formulation of I_t consists of "fast" and "slow" inactivation variables, with the relative contribution of the "slow" variable to overall inactivation being significantly larger in the endocardial model (≈42%), as opposed to the epicardial cell model (≈11%). Thus the equations for I_t are analogous with the general emerging consensus that I_t in rat consists of a fast component (thought to be generated principally by Kv4.2 and/or Kv4.3), and a slower component (thought to be primarily encoded by Kv1.4), with a greater contribution of the slower component in the endocardium (Wickenden et al., 1999b; Oudit et al., 2001).

The model also makes a contribution to the methodology for data analysis. It clearly demonstrates that when the slower component of I_t contributes significantly to the overall inactivation, as is the case in the endocardial cell, I_{peak} rather than $I_{peak} - I_{ss}$ is a more accurate measure of the recovery characteristics, as the latter underestimates the slower recovery and consequently fails to reproduce the prominent endocardial action potential rate dependence. This finding is important in the context of future experimental studies characterizing the recovery characteristics of I_t in pathophysiological conditions such as diabetes or thyroid hormone deficiencies (Shimoni et al., 1995) and hypertrophy (Volk et al., 2001), where the contributions of the slower component to the overall inactivation are enhanced.

Insight into the ionic mechanisms of the action potential plateau and the resting potential

The plateau phase of the endocardial action potential is more distinct and occurs at more depolarized potentials than in the epicardium. This results in a smaller "driving force" for I_{CaL} during the endocardial action potential. Driving force is defined as $V - E_{CaL}$, where V is the membrane potential. This contributes to the peak magnitude of I_{CaL} during the endocardial action potential, being smaller (−0.972 nA) than epicardial action potentials (−1.496 nA) (Fig. 10 *B*). During the endocardial action potential I_{CaL} also decays more slowly, as the membrane potential takes a longer time to reach the voltage at which I_{CaL} deactivates completely (≈−40 mV). This overall alteration in the temporal characteristics of I_{CaL} results in a larger influx of Ca^{2+} ions in the endocardial myocytes. Because the time constant for the activation of I_{ss} is 10 times slower than the corresponding one for I_t, a longer APD allows this current to activate to a greater extent and thus attain a higher peak magnitude underlying the endocardial action potential (125.6 pA), which is ≈3.3 times the peak value of I_{ss} underlying the epicardial action potential (37.79 pA). The interaction of I_B, I_{K1}, I_{NaK}, I_{CaP}, and I_{NaCa} is responsible for determining V_{rest} and R_{in}, which are quite similar in both cells on account of the uniform densities of these currents across the ventricular myocardium. However, I_{NaCa} underlying the endocardial action potential has a larger peak magnitude (−33.76 pA) compared with the epicardial action potential (−18.32 pA). This is due to the higher peak systolic $[Ca^{2+}]_i$ in the former. The time course of I_{NaCa} mimics the slow decay of the $[Ca^{2+}]_i$ in both cells. The "late" depolarizing effect of I_{NaCa} is opposed by I_{K1}, and their interaction underlies the slow final phase of repolarization observed in earlier experiments in rats (Schouten and ter Keurs, 1985).

APD and excitation-contraction coupling

The simulations for the epi and endocardial myocytes demonstrate that a longer APD can act as a significant inotropic variable in rat ventricular myocytes. Our model provides a straightforward explanation for this phenomenon by providing insight into the interaction of the ionic mechanisms that are responsible. A smaller density of I_t leads to a prolongation of the APD and alters the profile of I_{CaL}; in fact, Ca^{2+} influx is almost doubled during the endocardial AP. Initially, I_{NaCa} cannot extrude this surplus influx of Ca^{2+} ions, which leads to their uptake in the SR. As the SR Ca^{2+} content increases, the peak systolic value of $[Ca^{2+}]_i$ rises, which in turn increases I_{NaCa} until an equilibrium is reached, where the influx of Ca^{2+} ions via I_{CaL} (Q_{CaL}) and the efflux of Ca^{2+} ions via I_{NaCa} (Q_{NaCa}) are balanced. The APD, Q_{CaL}, Q_{NaCa}, peak systolic $[Ca^{2+}]_i$, $[Ca^{2+}]_{JSR}$, and peak magnitudes of I_{CaL} and I_{NaCa} have higher values in the endocardial cells than their respective counterparts in the epicardial cell (Tables 1 and 2). Thus our model provides a quantitative explanation, which is in agreement with previous experimental hypotheses (Bouchard et al., 1995; Clark et al., 1996), and recent experimental evidence for the mechanistic linkage between a prolonged APD and enhanced cardiac contractility (Sah et al., 2001). This process not only helps in explaining the heterogeneous nature of cell shortening in myocytes isolated from the rat left ventricle (Clark et al., 1993), but may also underlie the compensatory mechanism for the impaired cardiac contractility observed in the rat model of early stages of human heart failure (Wickenden et al., 1998) and myocardial infarction (Kaprielian et al., 1999), both conditions exhibiting a prolongation of the APD.

Limitations of the study

The primary limitation of the present rat model is that the description of the Ca^{2+} handling mechanism in the SR is adapted from an existing quantitative model of the canine midmyocardial ventricular cell (Winslow et al., 1999). Further modifications will be necessary to incorporate the rat-specific properties such as a prominent and longer-lasting rest potentiation and negative force-frequency characteristics (Bers, 2000). Second, recent experiments have suggested that the nature of depolarization-activated K^+ currents in rat myocytes is more complicated (Himmel et al.,

1999) than the simple K^+ current (I_t, I_{ss}) description in our model. As more quantitative data for these new components of outward K^+ currents become available, they can be incorporated into the model. The ionic concentrations in the extracellular bath are assumed to be constant; therefore, the rate dependence of the action potential does not take into account the possible accumulation of K^+ ions in a restricted extracellular or microanatomical (T-tubule system) space. Recent experiments suggest that I_{K1} exhibits non-uniform properties across the rat ventricle (Bryant et al., 1999; Yao et al., 1999). However, a more detailed study regarding the precise nature of these differences in density and their voltage-dependence is needed before it can be incorporated into the present models. Thus the possibility of other ionic currents contributing to the transmural dispersion of repolarization in the rat left ventricle cannot be ruled out.

CONCLUSION

We have developed comprehensive membrane action potential models for myocytes from the epi and endocardial regions of the adult rat left ventricle. These mathematical models are based on biophysical, experimentally derived descriptors of ionic currents and antiporters, and are able to accurately reproduce a wide variety of intrinsically heterogeneous properties associated with excitation, repolarization, and the excitation-contraction process in myocytes of epi and endocardial origin. The present study represents the first attempt to quantify and integrate the consequences of this transmural heterogeneity in the rat left ventricle. It demonstrates that the differential density and reactivation kinetics of the Ca^{2+}-independent transient outward K^+ current I_t contribute to the dispersion of repolarization (different waveforms), and suggests a mechanism for the regional differences in contractility in the ventricular myocardium. The different action potential waveforms result in ionic currents I_{CaL} and I_{ss}, along with the exchanger I_{NaCa} being significantly different in epi and endocardial myocytes. The resulting increase in the Ca^{2+} fluxes, which results in an increased SR Ca^{2+} load during the endocardial action potential, provides a plausible mechanistic linkage between prolonged APD and an increased inotropy.

Importantly, these simulations can serve as useful predictive tools for understanding the functional consequences of action potential alterations in rat models of different pathophysiological conditions such as diabetes (Shimoni et al., 1994, 1995), cardiac hypertrophy (Bryant et al., 1999; Volk et al., 2001), and myocardial infarction (Kaprielian et al., 1999; Yao et al., 1999). A consistent feature of each of these pathophysiological conditions is the downregulation of I_t. These changes are known to be very similar in humans and rats, suggesting that our model may be a useful adjunct for understanding these cardiac diseases in humans. The recent availability of genetically altered rats and their use in the molecular studies of the pathophysiology of cardiac disease (Franz et al., 1997; Lijnen and Petrov, 1999), and the fact that the rat remains one of the most commonly used mammalian models for drug development and screening (Budden et al., 1980; Cheung et al., 1993), adds considerable interest and utility for this model at present, and in the immediate future, as the model is extended and refined.

APPENDIX

Model formulation for the epicardial ventricular cell

Some fractional equations require evaluation of a limit to determine their values at membrane potentials for which their denominator is zero. Standard units (unless otherwise noted) are mV for membrane potential, nA for current, μS for conductance, mM s^{-1} for ionic flux, mM for ionic concentration, s for time constants, and s^{-1} for rate constants.

Membrane currents

Na^+ current, I_{Na}

$$I_{Na} = g_{Na} m^3 h j \, (V - E_{Na})$$

$$\bar{m} = \frac{1}{1 + e^{(v+45.0)/-6.5}}$$

$$\bar{h} = \bar{j} = \frac{1}{1 + e^{(v+76.1)/6.07}}$$

$$E_{Na} = \frac{RT}{F} \ln \frac{[Na^+]_o}{[Na^+]_i}$$

$$\frac{dm}{dt} = \frac{\bar{m} - m}{\tau_m}$$

$$\frac{dh}{dt} = \frac{\bar{h} - h}{\tau_h}$$

$$\frac{dj}{dt} = \frac{\bar{j} - j}{\tau_j}$$

$$\tau_m = \frac{0.00136}{\frac{0.32(V + 47.13)}{1.0 - e^{-0.1(V+47.13)}} + 0.08 e^{V/11}}$$

if $V \geq -40$ mV

$$\tau_h = 0.0004537(1.0 + e^{(V+10.66)/11.1})$$

$$\tau_j = \frac{0.01163(1.0 + e^{-0.1(V+32.0)})}{e^{-2.535 \times 10^{-7} V}}$$

else if $V \le -40$ mV

$$\tau_h = \frac{0.00349}{0.135e^{(V+80.0)/6.8} + 3.56e^{0.079V} + 3.1 \times 10^5 e^{0.35V}}$$

$$\tau_j = 0.00349 \div \left[\frac{V + 37.78}{1.0 + e^{0.311(V+79.23)}} (-127140e^{0.2444V} - 3.474 \times 10^{-5} e^{-0.04391V}) + \frac{0.1212e^{-0.01052V}}{1.0 + e^{-0.1378(V+40.14)}} \right]$$

L-type Ca^{2+} current I_{CaL}

$$I_{CaL} = g_{CaL} d \left[\left(0.9 + \frac{Ca_{inact}}{10.0} \right) f_{l1} + \left(0.1 - \frac{Ca_{inact}}{10.0} \right) f_{l2} \right] (V - E_{CaL})$$

$$\bar{d} = \frac{1}{1 + e^{(v+15.3)/-5.0}}$$

$$\bar{f}_{l1} = \bar{f}_{l2} = \frac{1}{1 + e^{(V+26.7)/5.4}}$$

$$E_{CaL} = 65.0$$

$$\tau_d = 0.00305e^{-0.0045(V+7.0)^2} + 0.00105e^{-0.002(V-18.0)^2} + 0.00025$$

$$\tau_{f_{l1}} = 0.105e^{-((V+45.0)/12.0)^2} + \frac{0.04}{(1.0 + e^{(-V+25.0)/25.0})} + \frac{0.015}{(1.0 + e^{(V+75.0)/25.0})} + 0.017$$

$$\tau_{f_{l2}} = 0.041e^{-((V+47.0)/12.0)^2} + \frac{0.08}{(1.0 + e^{(V+55.0)/-5.0})} + \frac{0.015}{(1.0 + e^{(V+75.0)/25.0})} + 0.017$$

$$\overline{Ca}_{inact} = \frac{1.0}{(1.0 + [Ca^{2+}]_{ss}/0.01)}$$

$$\tau_{Ca_{inact}} = 0.009$$

$$\frac{dd}{dt} = \frac{\bar{d} - d}{\tau_d}$$

$$\frac{df_{l1}}{dt} = \frac{\bar{f}_{l1} - f_{l1}}{\tau_{f_{l1}}}$$

$$\frac{df_{l2}}{dt} = \frac{\bar{f}_{l2} - f_{l2}}{\tau_{f2}}$$

$$\frac{dCa_{inact}}{dt} = \frac{\overline{Ca}_{inact} - Ca_{inact}}{\tau_{Ca_{inact}}}$$

Ca^{2+}-independent transient outward K^+ current, I_t

$$I_t = g_t r(as + bs_{slow})(V - E_K)$$

$$\bar{r} = \frac{1}{1 + e^{(V+10.6)/-11.42}}$$

$$\bar{s} = \bar{s}_{slow} = \frac{1}{1 + e^{(V+45.3)/6.8841}}$$

$$\tau_r = \frac{1.0}{45.16e^{0.03577(V+50.0)} + 98.9e^{-0.1(V+38.0)}}$$

$$\tau_s = 0.35e^{-(V+70.0/15.0)^2} + 0.035$$

$$\tau_{s_{slow}} = 3.7e^{-(V+70.0/30.0)^2} + 0.035$$

$$\frac{dr}{dt} = \frac{\bar{r} - r}{\tau_r}$$

$$\frac{ds}{dt} = \frac{\bar{s} - s}{\tau_s}$$

$$\frac{ds_{slow}}{dt} = \frac{\bar{s}_{slow} - s_{slow}}{\tau_{s_{slow}}}$$

$$E_K = \frac{RT}{F} \ln \frac{[K^+]_o}{[K^+]_i}$$

$$a = 0.886; \quad b = 0.114$$

Steady-state outward K^+ current, I_{ss}

$$I_{ss} = g_{ss} r_{ss} s_{ss} (V - E_K)$$

$$\bar{r}_{ss} = \frac{1}{1 + e^{(V+11.5)/-11.82}}$$

$$\bar{s}_{ss} = \frac{1}{1 + e^{(V+87.5)/10.3}}$$

$$\tau_{r_{ss}} = \frac{10.0}{45.16e^{0.03577(V+50.0)} + 98.9e^{-0.1(V+38.0)}}$$

$$\tau_{s_{ss}} = 2.1$$

$$\frac{dr_{ss}}{dt} = \frac{\bar{r}_{ss} - r_{ss}}{\tau_{r_{ss}}}$$

$$\frac{ds_{ss}}{dt} = \frac{\bar{s}_{ss} - s_{ss}}{\tau_{s_{ss}}}$$

Inward rectifier, I_{K1}

$$I_{K1} = \left[\frac{48}{(e^{(V+37)/25} + e^{(V+37)/-25})} + 10\right] \cdot \left[\frac{0.0001}{1 + e^{(V-E_K-76.77)/-17}}\right] + \frac{g_{K1}(V - E_K - 1.73)}{(1 + e^{1.613F((V-E_K-1.73)/RT)}) \cdot (1 + e^{[K^+]_o-0.9988/-0.124})}$$

Hyperpolarization-activated current, I_f

$$I_f = g_f\, y[f_{Na}(V - E_{Na}) + f_K(V - E_K)]$$

$$y_\infty = \frac{1}{1 + e^{(V+138.6)/10.48}}$$

$$f_{Na} = 0.2, \quad f_K = 1 - f_{Na}$$

$$\frac{dy}{dt} = \frac{y_\infty - y}{\tau_y}$$

$$\tau_y = \frac{1}{(0.11885e^{(V+80.00)/28.37} + 0.56236e^{(V+80.00)/-14.19})}$$

Background currents

$$I_{BNa} = g_{BNa}(V - E_{Na})$$

$$I_{BK} = g_{BK}(V - E_K)$$

$$I_{BCa} = g_{BCa}(V - E_{CaL})$$

$$I_B = I_{BNa} + I_{BCa} + I_{BK}$$

Na^+-K^+ pump current, I_{NaK}

$$I_{NaK} = \bar{I}_{NaK}\left(\frac{1.0}{1.0 + 0.1245e^{0.1VF/RT} + 0.0365\sigma e^{VF/RT}}\right) \cdot \left(\frac{[K^+]_o}{[K^+]_o + k_{m,K}}\right)$$

$$\sigma = \frac{e^{[Na^+]_o/67.3} - 1.0}{7.0}$$

Sarcolemmal Ca^{2+} pump current, I_{CaP}

$$I_{CaP} = \bar{I}_{CaP}\left(\frac{[Ca^{2+}]_i}{[Ca^{2+}]_i + 0.0004}\right)$$

Na^+-Ca^{2+} ion exchanger current, I_{NaCa}

$$I_{NaCa} = k_{NaCa}\{([Na^+]_i^3[Ca^{2+}]_o e^{(0.03743\gamma_{NaCa}V)} - [Na^+]_o^3[Ca^{2+}]_i e^{(0.03743(\gamma_{NaCa}-1)V)}) \div (1 + d_{NaCa}([Na^+]_o^3[Ca^{2+}]_i + [Na^+]_i^3[Ca^{2+}]_o)\}$$

Membrane potential

$$\frac{dV}{dt} = \frac{-(I_{Na} + I_{CaL} + I_t + I_{ss} + I_f + I_{K1} + I_B + I_{NaK} + I_{NaCa} + I_{CaP})}{C_m}$$

Ca^{2+} handling mechanisms

Calcium release channel in sarcoplasmic reticulum

$$\frac{dP_{C1}}{dt} = -k_a^+[Ca^{2+}]_{ss}^n P_{C1} + k_a^- P_{o1}$$

$$\frac{dP_{o1}}{dt} = k_a^+[Ca^{2+}]_{ss}^n P_{C1} - k_a^- P_{o1} - k_b^+[Ca^{2+}]_{ss}^m P_{o1} + k_b^- P_{o2} - k_c^+ P_{o1} + k_c^- P_{C2}$$

$$\frac{dP_{o2}}{dt} = k_b^+[Ca^{2+}]_{ss}^m P_{o1} - k_b^- P_{o2}$$

$$\frac{dP_{C2}}{dt} = k_c^+ P_{o1} - k_c^- P_{C2}$$

$$J_{rel} = \nu_1(P_{o1} + P_{o2})([Ca^{2+}]_{JSR} - [Ca^{2+}]_{ss})$$

SERCA2a Ca^{2+} pump

$$f_b = ([Ca^{2+}]_i/K_{fb})^{N_{fb}}$$

$$r_b = ([Ca^{2+}]_{NSR}/K_{rb})^{N_{rb}}$$

$$J_{up} = K_{SR}\frac{\nu_{maxf} f_b - \nu_{maxr} r_b}{1 + f_b + r_b}$$

Intracellular and sarcoplasmic reticulum Ca^{2+} fluxes

$$J_{tr} = \frac{[Ca^{2+}]_{NSR} - [Ca^{2+}]_{JSR}}{\tau_{tr}}$$

$$J_{xfer} = \frac{[Ca^{2+}]_{ss} - [Ca^{2+}]_i}{\tau_{xfer}}$$

$$J_{trpn} = \frac{d[HTRPNCa]}{dt} + \frac{d[LTRPNCa]}{dt}$$

$$\frac{d[HTRPNCa]}{dt} = k_{htrpn}^+[Ca^{2+}]_i([HTRPN]_{tot} - [HTRPNCa]) - k_{htrpn}^-[HTRPNCa]$$

$$\frac{d[LTRPNCa]}{dt} = k_{ltrpn}^+[Ca^{2+}]_i([LTRPN]_{tot} - [LTRPNCa]) - k_{ltrpn}^-[LTRPNCa]$$

Intracellular ion concentrations

$$\frac{d[Na^+]_i}{dt} = -(I_{Na} + I_{BNa} + 3I_{NaCa} + 3I_{NaK} + I_{f,Na})\frac{1.0}{V_{myo}F}$$

$$\frac{d[K^+]_i}{dt} = -(I_{ss} + I_{BK} + I_t + I_{K1} + I_{f,K} - 2I_{NaK})\frac{1.0}{V_{myo}F}$$

$$\frac{d[Ca^{2+}]_i}{dt} = \beta_i\left\{J_{xfer} - J_{up} - J_{trpn} - (I_{BCa} - 2I_{NaCa} + I_{CaP})\frac{1.0}{2V_{myo}F}\right\}$$

$$\beta_i = \left\{1 + \frac{[CMDN]_{tot}K_m^{CMDN}}{(K_m^{CMDN} + [Ca^{2+}]_i)^2} + \frac{[EGTA]_{tot}K_m^{EGTA}}{(K_m^{EGTA} + [Ca^{2+}]_i)^2}\right\}^{-1}$$

$$\beta_{ss} = \left\{1 + \frac{[CMDN]_{tot}K_m^{CMDN}}{(K_m^{CMDN} + [Ca^{2+}]_{ss})^2}\right\}^{-1}$$

$$\beta_{JSR} = \left\{1 + \frac{[CSQN]_{tot}K_m^{CSQN}}{(K_m^{CSQN} + [Ca^{2+}]_{JSR})^2}\right\}^{-1}$$

$$\frac{d[Ca^{2+}]_{ss}}{dt} = \beta_{ss}\left\{J_{rel}\frac{V_{JSR}}{V_{SS}} - J_{xfer}\frac{V_{myo}}{V_{SS}} - (I_{CaL})\frac{1.0}{2V_{ss}F}\right\}$$

$$\frac{d[Ca^{2+}]_{JSR}}{dt} = \beta_{JSR}\{J_{tr} - J_{rel}\}$$

$$\frac{d[Ca^{2+}]_{NSR}}{dt} = J_{up}\frac{V_{myo}}{V_{NSR}} - J_{tr}\frac{V_{JSR}}{V_{NSR}}$$

Model formulation for the endocardial ventricular cell

The endocardial action potential is formulated by making the following changes to the epicardial cell model parameters and equations.

Na^+ Current, I_{Na}

$$g_{Na,endo} = 1.33g_{Na,epi}$$

Ca^{2+}-independent Transient Outward K^+ Current, I_t

$$g_{i,endo} = 0.4647g_{t,epi}$$

$$\tau_{s,endo} = 0.55e^{-((V+70.0)/25.0)^2} + 0.049$$

$$\tau_{s_{slow},endo} = 3.3e^{-((V+70.0)/30.0)^2} + 0.049$$

$$a_{endo} = 0.583; \quad b_{endo} = 0.417$$

The authors gratefully acknowledge useful discussions with Dr. Anders Nygren (University of Calgary, Calgary, Alberta, Canada), Dr. Chris Ward (Queens University, Kingston, Ontario, Canada), and Chris Oehmen (Joint Graduate Program in Biomedical Engineering, The University of Memphis, and The University of Tennessee Health Science Center).

The authors acknowledge the support provided by the Whitaker Foundation (PI, S.S.D.), Herff Foundation Scholarship (S.V.P.), Alberta Heritage Foundation for Medical Research, Canadian Institutes of Health Research, and Heart and Stroke Foundation of Canada (PI, W.R.G.).

REFERENCES

Aggarwal, R., S. R. Shorofsky, L. Goldman, and C. W. Balke. 1997. Tetrodotoxin-blockable calcium currents in rat ventricular myocytes; a third type of cardiac cell sodium current. *J. Physiol.* 505:353–369.

Agus, Z. S., I. D. Dukes, and M. Morad. 1991. Divalent cations modulate the transient outward current in rat ventricular myocytes. *Am. J. Physiol.* 261:310–318.

Aiello, E. A., M. G. Petroff, A. R. Mattiazzi, and H. E. Cingolani. 1998. Evidence for an electrogenic Na^+-$HCO3^-$ symport in rat cardiac myocytes. *J. Physiol.* 512:137–148.

Antzelevitch, C., S. Sicouri, S. H. Litovsky, A. Lukas, S. C. Krishnan, J. Di Diego, G. A. Gintant, and D. W. Liu. 1991. Heterogeneity within the ventricular wall. Electrophysiology and pharmacology of epicardial, endocardial, and M cells. *Circ. Res.* 69:1427–1449.

Antzelevitch, C., G-X. Yan, W. Shimuzu, and A. Burashnikov. 1999. Electrical Heterogeneity, the ECG, and Cardiac Arrhythmias. *In* Cardiac Electrophysiology: From Cell to Bedside. D. P. Zipes and J. Jalife, editors. W. B. Saunders Co., Philadelphia. 222–238.

Apkon, M., and J. M. Nerbonne. 1991. Characterization of two distinct depolarization-activated K^+ currents in isolated adult rat ventricular myocytes. *J. Gen. Physiol.* 97:973–1011.

Ashamalla, S., D. Navarro, and C. A. Ward. 2001. Transmural gradient of sodium currents in rat left ventricle. *Biophys. J.* 80:224*a*. (abstr.).

Beeler, G. W., and H. Reuter. 1977. Reconstruction of the action potential of ventricular myocardial fibres. *J. Physiol.* 268:177–210.

Benitah, J. P., A. M. Gomez, P. Bailly, J. P. Da Ponte, G. Berson, C. Delgado, and P. Lorente. 1993. Heterogeneity of the early outward current in ventricular cells isolated from normal and hypertrophied rat hearts. *J. Physiol.* 469:111–138.

Berger, F., U. Borchard, D. Hafner, and T. M. Weis. 1998. Different inhibition patterns of tedisamil for fast and slowly inactivating transient outward current in rat ventricular myocytes. *Naunyn Schmiedebergs Arch. Pharmacol.* 357:291–298.

Bers, D. M. 2000. Calcium fluxes involved in control of cardiac myocyte contraction. *Circ. Res.* 87:275–281.

Bers, D. M., and E. Perez-Reyes. 1999. Ca channels in cardiac myocytes: structure and function in Ca influx and intracellular Ca release. *Cardiovasc. Res.* 42:339–360.

Bouchard, R. A., R. B. Clark, and W. R. Giles. 1995. Effects of action potential duration on excitation-contraction coupling in rat ventricular myocytes. Action potential voltage-clamp measurements. *Circ. Res.* 76:790–801.

Brahmajothi, M. V., D. L. Campbell, R. L. Rasmusson, M. J. Morales, J. S. Trimmer, J. M. Nerbonne, and H. C. Strauss. 1999. Distinct transient outward potassium current I_{to} phenotypes and distribution of fast-inactivating potassium channel alpha subunits in ferret left ventricular myocytes. *J. Gen. Physiol.* 113:581–600.

Bridge, J. H., J. R. Smolley, and K. W. Spitzer. 1990. The relationship between charge movements associated with I_{Ca} and $I_{Na\text{-}Ca}$ in cardiac myocytes. *Science.* 248:376–378.

Bryant, S. M., S. J. Shipsey, and G. Hart. 1997. Regional differences in electrical and mechanical properties of myocytes from guinea-pig hearts with mild left ventricular hypertrophy. *Cardiovasc. Res.* 35:315–323.

Bryant, S. M., S. J. Shipsey, and G. Hart. 1999. Normal regional distribution of membrane current density in rat left ventricle is altered in catecholamine-induced hypertrophy. *Cardiovasc. Res.* 42:391–401.

Budden, R., D. K. Detweiler, and G. Zbinden, editors. 1980. The Rat Electrocardiogram in Pharmacology and Toxicology. Pergamon Press, Oxford.

Campbell, D. L., R. L. Rasmusson, M. B. Comer, and H. C. Strauss. 1995. The cardiac calcium-independent transient outward potassium current: kinetics, molecular properties, and role in ventricular repolarization. *In* Cardiac Electrophysiology: From Cell to Bedside. D. P. Zipes, and J. Jalife, editors. W. B. Saunders Co., Philadelphia. 83–96.

Casis, O., M. Gallego, M. Iriarte, and J. A. Sanchez-Chapula. 2000. Effects of diabetic cardiomyopathy on regional electrophysiologic characteristics of rat ventricle. *Diabetologia.* 43:101–109.

Casis, O., M. Iriarte, M. Gallego, and J. A. Sanchez-Chapula. 1998. Differences in regional distribution of K^+ current densities in rat ventricle. *Life Sci.* 63:391–400.

Cerbai, E., M. Barbieri, Q. Li, and A. Mugelli. 1996. Occurrence and properties of the hyperpolarization-activated current I_f in ventricular myocytes from normotensive and hypertensive rats during aging. *Circulation.* 94:1674–1681.

Cheung, P. H., M. K. Pugsley, and M. J. Walker. 1993. Arrhythmia models in the rat (Review). *J. Pharmacol. Toxicol. Methods.* 29:179–184.

Clark, R. B., R. A. Bouchard, and W. R. Giles. 1996. Action potential duration modulates calcium influx, Na^+-Ca^{2+} exchange, and intracellular calcium release in rat ventricular myocytes. *Ann. N.Y. Acad. Sci.* 779:417–428.

Clark, R. B., R. A. Bouchard, E. Salinas-Stefanon, J. Sanchez-Chapula, and W. R. Giles. 1993. Heterogeneity of action potential waveforms and potassium currents in rat ventricle. *Cardiovasc. Res.* 27:1795–1799.

Clark, R. B., J. Sanchez-Chapula, E. Salinas-Stefanon, H. J. Duff, and W. R. Giles. 1995. Quinidine-induced open channel block of K^+ current in rat ventricle. *Br. J. Pharmacol.* 115:335–343.

Colatsky, T. J. 1980. Voltage clamp measurements of sodium channel properties in rabbit cardiac Purkinje fibres. *J. Physiol.* 305:215–234.

Demir, S. S., R. J. Butera, A. A. DeFranceschi, J. W. Clark, and J. H. Byrne. 1997. Phase sensitivity and entrainment in a modeled bursting neuron. *Biophys. J.* 72:579–594.

Demir, S. S., J. W. Clark, and W. R. Giles. 1999. Parasympathetic modulation of sinoatrial node pacemaker activity in rabbit heart: a unifying model. *Am. J. Physiol. Heart Circ. Physiol.* 276:H2221–H2244.

Demir, S. S., J. W. Clark, C. R. Murphey, and W. R. Giles. 1994. A mathematical model of a rabbit sinoatrial node cell. *Am. J. Physiol. Cell Physiol.* 266:C832–C852.

Diochot, S., M. D. Drici., D. Moinier, M. Fink, and M. Lazdunski. 1999. Effects of phrixotoxins on the Kv4 family of potassium channels and implications for the role of I_{to1} in cardiac electrogenesis. *Br. J. Pharmacol.* 126:251–263.

Eddlestone, G. T., A. C. Zygmunt, and C. Antzelevitch. 1996. Larger late sodium current contributes to the longer action potential of the M-cell in canine ventricular myocardium. *PACE.* 19:569*a*. (Abstr.).

Fares, N., P. Bois, J. Lenfant, and D. Potreau. 1998. Characterization of a hyperpolarization-activated current in dedifferentiated adult rat ventricular cells in primary culture. *J. Physiol.* 506:73–82.

Fedida, D., and W. R. Giles. 1991. Regional variations in action potentials and transient outward current in myocytes isolated from rabbit left ventricle. *J. Physiol.* 442:191–209.

Figueredo, V. M., R. Brandes, M. W. Weiner, B. M. Massie, and S. A. Camacho. 1993. Endocardial versus epicardial differences of intracellular free calcium under normal and ischemic conditions in perfused rat hearts. *Circ. Res.* 72:1082–1090.

Fiset, C., R. B. Clark, T. S. Larsen, and W. R. Giles. 1997b. A rapidly activating sustained K^+ current modulates repolarization and excitation-contraction coupling in adult mouse ventricle. *J. Physiol.* 504: 557–563.

Fiset, C., R. B. Clark, Y. Shimoni, and W. R. Giles. 1997a. *Shal*-type channels contribute to the Ca^{2+}-independent transient outward K^+ current in rat ventricle. *J. Physiol.* 500:51–64.

Franz, M. R., K. Bargheer, W. Rafflenbeul, A. Haverich, and P. R. Lichtlen. 1987. Monophasic action potential mapping in human subjects with normal electrocardiograms: direct evidence for the genesis of the T wave. *Circulation.* 75:379–386.

Franz, W. M., O. J. Mueller, R. Hartong, N. Frey, and H. A. Katus. 1997. Transgenic animal models: new avenues in cardiovascular physiology. *J. Mol. Med.* 75:115–129.

Giles, W. R., R. B. Clark, and A. P. Braun. 1996. Ca^{2+}-independent transient outward K^+ current in mammalian heart. *In* Molecular Physiology and Pharmacology of Cardiac Ion Channels and Transporters. M. Morad, Y. Kurachi, A. Noma, and M. Hosada, editors. Kluwer Press Ltd., Amsterdam. 141–168.

Gomez, A. M., J. P. Benitah, D. Henzel, A. Vinet, P. Lorente, and C. Delgado. 1997. Modulation of electrical heterogeneity by compensated hypertrophy in rat left ventricle. *Am. J. Physiol. Heart Circ. Physiol.* 272:H1078–H1086.

Guo, W., H. Xu, B. London, and J. M. Nerbonne. 1999. Molecular basis of transient outward K^+ current diversity in mouse ventricular myocytes. *J. Physiol.* 521:587–599.

Gussak, I., B. R. Chaitman, S. L. Kopecky, and J. M. Nerbonne. 2000. Rapid ventricular repolarization in rodents: electrocardiographic manifestations, molecular mechanisms, and clinical insights. *J. Electrocardiol.* 33:159–170.

Han, S., A. Schiefer, and G. Isenberg. 1994. Ca^{2+} load of guinea-pig ventricular myocytes determines efficacy of brief Ca^{2+} currents as trigger for Ca^{2+} release. *J. Physiol.* 480:411–421.

Hanck, D. A. 1995. Biophysics of sodium channels. *In* Cardiac Electrophysiology: From Cell to Bedside. D. P. Zipes and J. Jalife, editors. W. B. Saunders Co., Philadelphia. 65–74.

Himmel, H. M., E. Wettwer, Q. Li, and U. Ravens. 1999. Four different components contribute to outward current in rat ventricular myocytes. *Am. J. Physiol. Heart Circ. Physiol.* 277:H107–H118.

Hodgkin, A. L., and A. F. Huxley. 1952. A quantitative description of membrane current and its application to conduction and excitation in nerve. *J. Physiol.* 117:500–544.

Kaprielian, R., A. D. Wickenden, Z. Kassiri, T. G. Parker, P. P. Liu, and P. H. Backx. 1999. Relationship between K^+ channel down-regulation and $[Ca^{2+}]_i$ in rat ventricular myocytes following myocardial infarction. *J. Physiol.* 517:229–245.

Katsube, Y., H. Yokoshiki, L. Nguyen, M. Yamamoto, and N. Sperelakis. 1998. L-type Ca^{2+} currents in ventricular myocytes from neonatal and adult rats. *Can. J. Physiol. Pharmacol.* 76:873–881.

Kimura, S., A. L. Bassett, T. Furukawa, J. Cuevas, and R. J. Myerburg. 1990. Electrophysiological properties and responses to simulated ischemia in cat ventricular myocytes of endocardial and epicardial origin. *Circ. Res.* 66:469–477.

Lee, H. C., T. Lu, N. L. Weintraub, M. VanRollins, A. A. Spector, and E. F. Shibata. 1999. Effects of epoxyeicosatrienoic acids on the cardiac sodium channels in isolated rat ventricular myocytes. *J. Physiol.* 519: 153–168.

Lijnen, P., and V. Petrov. 1999. Renin-angiotensin system, hypertrophy and gene expression in cardiac myocytes (Review). *J. Mol. Cell. Cardiol.* 31:949–970.

Lindblad, D. S., C. R. Murphey, J. W. Clark, and W. R. Giles. 1996. A model of the action potential and underlying membrane currents in a rabbit atrial cell. *Am. J. Physiol. Heart Circ. Physiol.* 271: H1666–H1696.

Liu, D. W., and C. Antzelevitch. 1995. Characteristics of the delayed rectifier current (I_{Kr} and I_{Ks}) in canine ventricular epicardial, midmyocardial, and endocardial myocytes. A weaker I_{Ks} contributes to the longer action potential of the M cell. *Circ. Res.* 76:351–365.

Luo, C. H., and Y. Rudy. 1994. A dynamic model of the cardiac ventricular action potential. I. Simulation of ionic currents and concentration changes. *Circ. Res.* 74:1071–1096.

MacDonell, K. L., D. L. Severson, and W. R. Giles. 1998. Depression of excitability by sphingosine 1-phosphate in rat ventricular myocytes. *Am. J. Physiol. Heart Circ. Physiol.* 275:H2291–H2299.

Main, M. C., S. M. Bryant, and G. Hart. 1998. Regional differences in action potential characteristics and membrane currents of guinea-pig left ventricular myocytes. *Exp. Physiol.* 83:747–761.

McCall, E., K. S. Ginsburg, R. A. Bassani, T. R. Shannon, M. Qi, A. M. Samarel, and D. M. Bers. 1998. Ca flux, contractility, and excitation-contraction coupling in hypertrophic rat ventricular myocytes. *Am. J. Physiol. Heart Circ. Physiol.* 274:H1348–H1360.

Meszaros, J., J. J. Coutinho, S. M. Bryant, K. O. Ryder, and G. Hart. 1997. L-type calcium current in catecholamine-induced cardiac hypertrophy in the rat. *Exp. Physiol.* 82:71–83.

Nabauer, M., D. Beuckelmann, P. Uberfuhr, and G. Steinbeck. 1996. Regional differences in current density and rate dependence properties of the transient outward current in subepicardial and subendocardial myocytes of human left ventricle. *Circulation.* 93:168–177.

Nawrath, H., and J. W. Wegener. 1997. Kinetics and state-dependent effects of verapamil on cardiac L-type calcium channels. *Naunyn Schmiedebergs Arch. Pharmacol.* 55:79–86.

Nguyen-Tran, V. T., S. W. Kubalak, S. Minamisawa, C. Fiset, S. Minamisawa, K. C. Wollert, A. B. Brown, P. Ruiz-Lozano, S. Barrere-Lemaire, R. Kondo, L. W. Norman, R. G. Gourdie, M. M. Rahme, G. K. Feld, R. B. Clark, W. R. Giles, and K. R. Chien. 2000. A novel genetic pathway for sudden cardiac death via defects in the transition between ventricular and conduction system cell lineages. *Cell.* 102:671–682.

Noble, D., A. Varghese, P. Kohl, and P. Noble. 1998. Improved guinea-pig ventricular cell model incorporating a diadic space, I_{Kr} and I_{Ks}, and length- and tension-dependent processess. *Can. J. Cardiol.* 14:123–134.

Nordin, C. 1993. Computer model of membrane current and intracellular Ca^{2+} flux in the isolated guinea pig ventricular myocyte. *Am. J. Physiol. Heart Circ. Physiol.* 265:H2117–H2136.

Nygren, A., C. Fiset, L. Firek, J. W. Clark, D. S. Lindblad, and W. R. Giles. 1998. Mathematical model of an adult human atrial cell. The role of K^+ currents in repolarization. *Circ. Res.* 82:63–81.

Oehmen, C. 1999. Parameter sensitivity studies of various cardiac channels. M.S. Thesis, University of Tennessee, Memphis.

Oudit, G. Y., Z. Kassiri, R. Sah, R. J. Ramirez, C. Zobel, and P. H. Backx. 2001. The molecular physiology of the cardiac transient outward potassium current I_{to} in normal and diseased myocardium. *J. Mol. Cell. Cardiol.* 33:851–872.

Page, E. 1978. Quantitative ultrastructural analysis in cardiac membrane physiology. *Am. J. Physiol. Cell Physiol.* 235:C147–C158.

Pond, A. L., B. K. Scheve, A. T. Benedict, K. Petrecca, D. R. Van Wagoner, A. Shrier, and J. M. Nerbonne. 2000. Expression of distinct ERG proteins in rat, mouse, and human heart. Relation to functional I_{Kr} channels. *J. Biol. Chem.* 275:5997–6006.

Priebe, L., and D. Beuckelmann. 1998. Simulation study of cellular electric properties in heart failure. *Circ. Res.* 82:1206–1223.

Qin, D., Z. H. Zhang, E. B. Caref, M. Boutjdir, P. Jain, and N. el-Sherif. 1996. Cellular and ionic basis of arrhythmias in postinfarction remodeled ventricular myocardium. *Circ. Res.* 79:461–473.

Richard, S., P. Charnet, and J. M. Nerbonne. 1993. Interconversion between distinct gating pathways of the high threshold calcium channel in rat ventricular myocytes. *J. Physiol.* 462:197–228.

Riemer, T. L., E. A. Sobie, and L. Tung. 1998. Stretch-induced changes in arrhythmogenesis and excitability in experimentally based heart cell models. *Am. J. Physiol. Heart Circ. Physiol.* 275:H431–H442.

Sah, R, R. J. Ramirez, R. Kaprielian, and P. H. Backx. 2001. Alterations in action potential profile enhance excitation-contraction coupling in rat cardiac myocytes. *J. Physiol.* 533:201–214.

Saint, D. A., Y. K. Ju, and P. W. Gage. 1992. A persistent sodium current in rat ventricular myocytes. *J. Physiol.* 453:219–231.

Satoh, H., L. M. Delbridge, L. A. Blatter, and D. M. Bers. 1996. Surface-volume relationship in cardiac myocytes studied with confocal microscopy and membrane capacitance measurements: species-dependence and developmental effects. *Biophys. J.* 70:1494–1504.

Schaper, J., E. Meiser, and G. Stammler. 1985. Ultrastructural morphometric analysis of myocardium from dogs, rats, hamsters, mice, and from human hearts. *Circ. Res.* 56:377–391.

Schouten, V. J., and H. E. ter Keurs. 1985. The slow repolarization phase of the action potential in rat heart. *J. Physiol.* 360:13–25.

Sham, J. S., S. N. Hatem, and M. Morad. 1995. Species differences in the activity of the Na^+-Ca^{2+} exchanger in mammalian cardiac myocytes. *J. Physiol.* 488:623–631.

Shimoni, Y., L. Firek, D. Severson, and W. R. Giles. 1994. Short-term diabetes alters K^+ currents in rat ventricular myocytes. *Circ. Res.* 74:620–628.

Shimoni, Y., D. Severson, and W. R. Giles. 1995. Thyroid status and diabetes modulate regional differences in potassium currents in rat ventricle. *J. Physiol.* 488:673–688.

Shipsey, S. J., S. M. Bryant, and G. Hart. 1997. Effects of hypertrophy on regional action potential characteristics in the rat left ventricle: a cellular basis for T-wave inversion? *Circulation.* 96:2061–2068.

Sicouri, S., and C. Antzelevitch. 1991. A subpopulation of cells with unique electrophysiological properties in the deep subepicardium of the canine ventricle. The M cell. *Circ. Res.* 68:1729–1741.

Sicouri, S., M. Quist, and C. Antzelevitch. 1996. Evidence for the presence of M cells in the guinea pig ventricle. *J. Cardiovasc. Electrophysiol.* 7:503–511.

Spencer, C. I., W. Uchida, and R. Z. Kozlowski. 2000. A novel anionic conductance affects action potential duration in isolated rat ventricular myocytes. *Br. J. Pharmacol.* 129:235–238.

Stengl, M., E. Carmeliet, K. Mubagwa, and W. Flameng. 1998a. Modulation of transient outward current by extracellular protons and Cd^{2+} in rat and human ventricular myocytes. *J. Physiol.* 511:827–836.

Stengl, M., K. Mubagwa, E. Carmeliet, and W. Flameng. 1998b. Phenylephrine-induced stimulation of Na^+/Ca^{2+} exchange in rat ventricular myocytes. *Cardiovasc. Res.* 38:703–710.

Stimers, J. R., and M. Dobretsov. 1998. Adrenergic stimulation of Na/K pump current in adult rat cardiac myocytes in short-term culture. *J. Membr. Biol.* 163:205–216.

Sun, L., J. S. Fan, J. W. Clark, and P. T. Palade. 2000. A model of the L-type Ca^{2+} channel in rat ventricular myocytes: ion selectivity and inactivation mechanisms. *J. Physiol.* 529:139–158.

Trafford, A. W., M. E. Diaz, and D. A. Eisner. 2001. Coordinated control of cell Ca^{2+} loading and triggered release from the sarcoplasmic reticulum underlies the rapid inotropic response to increased L-type Ca^{2+} current. *Circ. Res.* 88:195–201.

Volk, T., T. H. Nguyen, J. H. Schultz, and H. Ehmke. 1999. Relationship between transient outward K^+ current and Ca^{2+} influx in rat cardiac myocytes of endo- and epicardial origin. *J. Physiol.* 519: 841–850.

Volk, T., T. H. Nguyen, J. H. Schultz, J. Faulhaber, and H. He. 2001. Regional alterations of repolarizing K^+ currents among the left ventricular free wall of rats with ascending aortic stenosis. *J. Physiol.* 530: 443–455.

Wallert, M. A., and O. Frohlich. 1989. Na^+-H^+ exchange in isolated myocytes from adult rat heart. *Am. J. Physiol. Cell Physiol.* 257: C207–C213.

Ward, C. A., Z. Ma, S. S. Lee, and W. R. Giles. 1997. Potassium currents in atrial and ventricular myocytes from a rat model of cirrhosis. *Am. J. Physiol. Gastrointest. Liver Physiol.* 273:G537–G544.

Watanabe, T., L. M. Delbridge, J. O. Bustamante, and T. F. McDonald. 1983. Heterogeneity of the action potential in isolated rat ventricular myocytes and tissue. *Circ. Res.* 52:280–290.

Weis, T., F. Berger, and U. Borchard. 1993. A slowly inactivating transient outward current in rat ventricular myocytes. *Pflugers. Arch.* 425: 184–186.

Wettwer, E., G. Amos, J. Gath, H. R. Zerkowski, J. C. Reidemeister, and U. Ravens. 1993. Transient outward current in human and rat ventricular myocytes. *Cardiovasc. Res.* 27:1662–1669.

Wickenden, A. D., T. J. Jegla, R. Kaprielian, and P. H. Backx. 1999b. Regional contributions of Kv1.4, Kv4.2, and Kv4.3 to transient outward K^+ current in rat ventricle. *Am. J. Physiol. Heart Circ. Physiol.* 276: H1599–H1607.

Wickenden, A. D., R. Kaprielian, Z. Kassiri, J. N. Tsoporis, R. Tsushima, G. I. Fishman, and P. H. Backx. 1998. The role of action potential prolongation and altered intracellular calcium handling in

the pathogenesis of heart failure (Review). *Cardiovasc. Res.* 37: 312–323.

Wickenden, A. D., R. Tsushima, V. A. Losito, R. Kaprielian, and P. H. Backx. 1999a. Effects of Cd^{2+} on Kv4.2 and Kv1.4 expressed in Xenopus oocytes and on the transient outward currents in rat and rabbit ventricular myocytes. *Cell. Physiol. Biochem.* 9:11–28.

Winslow, R. L., J. Rice, S. Jafri, E. Marban, and B. O'Rourke. 1999. Mechanisms of altered excitation-contraction coupling in canine tachycardia-induced heart failure. II. Model studies. *Circ. Res.* 84: 571–586.

Yao, J. A., M. Jiang, J. S. Fan, Y. Y. Zhou, and G. N. Tseng. 1999. Heterogeneous changes in K currents in rat ventricles three days after myocardial infarction. *Cardiovasc. Res.* 44:132–145.

Zygmunt, A. C., R. J. Goodrow, and C. Antzelevitch. 2000. I_{NaCa} contributes to electrical heterogeneity within the canine ventricle. *Am. J. Physiol. Heart Circ. Physiol.* 278:H1671–H1678.